EFFECTS OF SCALE AND STABILITY ON LARGE-SCALE PRECIPITATION

by

DAVID ARTHUR OLSON

B.S., University of Massachusetts
(1958)

SUBMITTED IN PARTIAL FULFILLMENT
OF THE REQUIREMENTS FOR THE
DEGREE OF
MASTER OF SCIENCE
at the
MASSACHUSETTS INSTITUTE OF
TECHNOLOGY
August 1965

Signature of Author.....
Department of Meteorology, August 23, 1965

Certified by.....
Thesis Supervisor

Accepted by.....
Chairman, Departmental Committee on Graduate Students

EFFECTS OF SCALE AND STABILITY ON LARGE-SCALE PRECIPITATION

by

David Arthur Olson

Submitted to the Department of Meteorology
on August 23, 1965 in partial fulfillment of the requirement
for the Degree of Master of Science

ABSTRACT

Most cloud and precipitation models have been incapable of predicting adequate amounts of precipitation. This primarily is due to the effect on the vertical motion of the latent heat of condensation.

In this work, a theoretical enhancement factor is presented. This factor is the ratio of the vertical motion including the latent heat effect to that without this effect. Horizontal scale and vertical stability are the parameters determining this factor.

It is assumed that this ratio of vertical motions is equivalent to the ratio of observed to predicted mean precipitation data. Predicted rainfall does not include the latent heat effect. The theoretical enhancement factors are compared to the empirical precipitation ratios for several storms. A correlation of 0.83 is observed. For large-scale winter storms, it is concluded that stability is the important parameter. Finally, thickness dependent enhancement factors are presented for use in conjunction with the current precipitation model at the National Meteorological Center.

Thesis Supervisor: Frederick Sanders

Title: Associate Professor of Meteorology

ACKNOWLEDGEMENT

The author is indebted to Professor Frederick Sanders for his inspiration, guidance, and encouragement during the preparation of this thesis.

Acknowledgement is made to the U. S. Weather Bureau National Meteorological Center at Suitland, Maryland for providing some of the necessary material and to Miss Ann Corrigan for plotting some of the necessary diagrams.

TABLE OF CONTENTS

LIST OF FIGURES

---

* The 24-hour periods end at 1200GMT on the following dates:

December 4, 1964
December 11, 1964
December 12, 1964
December 18, 1964
January 8, 1965
January 9, 1965
January 22, 1965
January 23, 1965
February 9, 1965
February 10, 1965
February 25, 1965
March 2, 1965
March 10, 1965
March 18, 1965
April 12, 1965
April 16, 1965

I. INTRODUCTION

After the high-speed computer was adopted for solution of meteorological problems(e. g., prediction of pressure and wind fields), numerical models for the prediction of cloud and precipitation were developed. The early ones [Thompson and Collins(1953), Spar(1953), Kuhn(1953), Collins and Kuhn(1954), Swayne(1956), Estoque(1957)] showed that large-scale vertical motion could be employed as a primary predictor of cloud and precipitation. These schemes failed to predict adequate quantities of precipitation. However, areal distribution forecasts were moderately successful. These models used only limited moisture fields and the vertical motions were occasionally inconsistent with the pressure distribution.

The importance of the release of latent heat in quantitative precipitation forecasting was noted by Smebye(1958), Smagorinsky and Collins(1955), Staff Members of Tokyo University(1955), Smagorinsky (1956), and Aubert(1957). They observed the latent heat effect to produce vertical motions the same order of magnitude as those predicted with the exclusion of latent heat. Danard(1964) and Smagorinsky(1956) observed the size of the predicted area to decrease slightly from the effects of latent heat.

Youmkin, LaRue, and Sanders(1965) developed the model currently in use at the National Meteorological Center. The effect of latent heat is not explicitly included. As a result, this model also is deficient in

its quantitative predictions.

Vertical motion is normally predicted by assuming dry adiabatic motion and neglecting diabatic sources of heating. This results in a vertical motion field which is used as a primary predictor of large-scale precipitation. The condensation necessary to produce this precipitation releases latent heat. This heat enhances the vertical motion and, as a consequence, the precipitation.

Theoretical considerations indicate that the latent heat effect may be explained in terms of vertical stability and horizontal scale. The purpose of this work is to investigate both theoretically and experimentally the effects of scale and stability to determine a best enhancement factor to be used operationally in the SLYH[1] model predictions. It is assumed that condensation equals precipitation, moist to dry model vertical motion ratios are equivalent to observed to forecast precipitation ratios, and released latent heat enhances local vertical motion.

---

[1] The Younkin, LaRue, and Sanders model shall hereafter be referred to as the SLYH model.

II. THEORETICAL FORMULATIONS

The primary purpose of this work is to improve SLYH model forecasts. The theoretical scheme of this model[2] is formulated in a (x, y, σ, t)-coordinate system, where $\sigma = p/\pi$, π is surface pressure, and p, the pressure at any level. Expressions for the conservation of virtual specific humidity, q, and the conservation of mass are manipulated to yield a prediction equation for virtual precipitable water, W':

$$(1)\quad \frac{\partial W'}{\partial t} = \frac{\pi}{g}\int_0^1 (-\underset{\sim}{V}\cdot\nabla q)\,d\sigma + \frac{\pi}{g}\int_0^1 (-q\,\nabla\cdot\underset{\sim}{V})\,d\sigma + \frac{1}{g}\int_0^1 (-q\,\underset{\sim}{V}\cdot\nabla\pi)\,d\sigma$$

Introduction of modeling parameters from climatological wind and moisture data leads to:

$$(2)\quad \frac{\partial W'}{\partial t} = -(K_1\underset{\sim}{V}_1 + K_2\underset{\sim}{\bar{V}})\cdot\nabla w - \frac{wK_3}{\pi}\omega_m + \frac{w\sigma_m K_3}{\pi}\underset{\sim}{\bar{V}}\cdot\nabla\pi + \frac{w}{\pi}(1+\sigma_m K_3)\frac{\partial\pi}{\partial t},$$

where W is precipitable water, the K's are constants derived from climatological data, $\underset{\sim}{\bar{V}}$ is the mean wind, $\underset{\sim}{V}_1$ is the wind at the level $\sigma = 1$, the subscript m refers to the σ-surface where $\underset{\sim}{V} = \underset{\sim}{\bar{V}}$, and $\omega = dp/dt$. σ will be used no further in this sense.

T The following operational model would be equivalent to the theoretical if a uniform surface pressure of 1000-mb is assumed everywhere. This is unrealistic, so the operational model is only related to the theoretical. The parameters used operationally are the surface to 500-mb precipitable water and the initial and prognostic 1000-mb and 500-mb height and wind fields, as obtained from the

---

[2] The complete derivation is contained in Younkin, LaRue, and Sanders(1965).

baroclinic 3-level and the Reed (1963) model 1000-mb forecasts.

First, the prediction equation is rewritten as:

(3) $$\frac{\partial W'}{\partial t} = -\underset{\sim}{V}_* \cdot \nabla W - \frac{W h_3}{1000\,mb}\omega_m + \frac{W \sigma_m h_3}{1000\,mb}\underset{\sim}{V}_3 \cdot \nabla \pi,$$

(4) where $$\underset{\sim}{V}_* = K_1\underset{\sim}{V}_0 + K_2\underset{\sim}{V}_5,$$

with $\underset{\sim}{V}_0$ and $\underset{\sim}{V}_5$ being the 1000-mb and 500-mb winds, respectively. The observed precipitable water is converted to a saturation thickness, h_s, which is defined by Younkin, LaRue, and Sanders(1965) as the thickness of a 1000- to 500-mb layer with a uniform 70% relative humidity, a moist-adiabatic lapse rate, and a mass of water vapor equal to the observed precipitable water. It is now time to introduce the saturation deficit, h_d, which is defined by:

(5) $$h_d = h_5 - h_s,$$

where h_5 is the observed 1000- to 500-mb thickness. This yields an estimate of the degree of saturation.

Further manipulation and the introduction of modeling parameters leads to:

(6) $$\frac{\partial h_d}{\partial t} = -\underset{\sim}{V}_* \cdot \nabla h_d + 2\frac{Dh_5}{Dt} - (0.41\underset{\sim}{V}_0 + 0.59\underset{\sim}{V}_3)\cdot \nabla P,$$

(7) where $$P \approx 800\left(\frac{\pi}{1000\,mb} - 1\right) M.$$

From here the prediction equation becomes:

(8) $$\frac{D}{Dt}(h_d + P - 2h_5) = 0,$$

(9) where $$\frac{D}{Dt} = \frac{\partial}{\partial t} + \underset{\sim}{V}_* \cdot \nabla,$$

(10) and $$\underset{\sim}{V}_* = K_1\underset{\sim}{V}_0 + K_2\underset{\sim}{V}_5.$$

K_1, K_2 and the coefficient '2' from Eq. (8) are constants calculated from climatological vertical profiles of wind, specific humidity, and

potential temperature and from an assumed profile of divergence.

The quantity being predicted here is the saturation deficit For an example, see Younkin, LaRue, and Sanders(1965) . From the previous definition, a saturation deficit forecast of zero implies a column of air with a 70& relative humidity. The area of precipitation is outlined by the zero isopleth of saturation deficit. Negative saturation deficits which accumulate along trajectories are regarded as precipitation, which is deposited at the ends of the trajectories. The quantitative precipitation forecast is derived from the predicted saturation deficit through use of the table in the Appendix.

Early models were plagues by problems arising from use of inadequate moisture fields, by using vertical motion fields inconsistent with surface circulations, or by being non-adaptable to numerical solution. The SLYH model overcomes these by letting consistent time-integrated fields of motion operate on vertically integrated moisture fields. Despite this, predicted rainfall amounts verify well below the observed.

The release of latent heat of condensation is a source of diabatic heating, which influences the local vertical motion. According to Younkin[3], for a first effort at the National Meteorological Center predicted amounts were simply enhanced by a factor of 3. This led to overprediction at high latitudes and an underprediction at lower

---

[3] Younkin, personal communication.

latitudes. This suggested a thickness dependence. A thickness dependent factor was adopted from empirical considerations, showing some improvement.

The SLYH model is derived from consideration of dry adiabatic motion, that is, it excludes the effects of the presence of moisture. By neglecting all sources of heating in the thermodynamic equation:

$$(11) \qquad \frac{d\theta}{dt} = 0 = \frac{\partial \theta}{\partial t} + \underset{\sim}{V} \cdot \nabla \theta + \omega \frac{\partial \theta}{\partial p},$$

where θ is potential temperature, one may combine this with the vorticity equation for quasi-qeostrophic motion to obtain the usual form of the ω-equation:

$$(12) \qquad \left(\sigma \nabla^2 + f_0^2 \frac{\partial^2}{\partial p^2} \right) \omega_0 = - f_0 \frac{\partial}{\partial p} \left(-\underset{\sim}{V} \cdot \nabla \eta \right) + \nabla^2 \left(-\underset{\sim}{V} \cdot \nabla \frac{\partial \Phi}{\partial p} \right),$$

where Φ is the geopotential, η is the absolute vorticity, f_0 is the coriolis parameter, and σ is the static stability not to be confused with σ of Eq. (1) . The stability is a function of pressure as defined by:

$$(13) \qquad \sigma = \frac{\partial \ln \theta}{\partial p} \frac{\partial \Phi}{\partial p} = - \frac{RT}{\theta p} \frac{\partial \theta}{\partial p}.$$

The procedure for the development of the ω-equation (12) is the same as the procedure used in the following to obtain a "moist" ω-equation. First, a source of diabatic heating is introduced into the thermodynamic equation:

$$(14) \qquad \frac{d\theta}{dt} = \frac{\theta}{c_p T} \frac{dQ}{dt} = \frac{\partial \theta}{\partial t} + \underset{\sim}{V} \cdot \nabla \theta + \omega \frac{\partial \theta}{\partial p},$$

where c_p is the specific heat of dry air at constant pressure, T is temperature, and dQ/dt is the rate of heating. Taking the release of latent heat as the heating source:

(15) $$\frac{dQ}{dt} = L\left(\frac{dq_w}{dp}\right)_{MA}\omega,$$

L being the latent heat of condensation, and $\left(\frac{dq_w}{dp}\right)_{MA}$ the change of saturation mixing ratio along a moist adiabat. Substitution of (15) into (14) and combining the coefficients of ω leads to:

(16) $$0 = \frac{\partial\theta}{\partial t} + \underset{\sim}{V}\cdot\nabla\theta + \omega\left[\frac{\partial\theta}{\partial p} - \frac{\theta L}{c_p T}\left(\frac{dq_w}{dp}\right)_{MA}\right].$$

The potential temperature is defined by:

(17) $$\theta = T\left(\frac{1000\ mb}{p}\right)^{\kappa}$$

Applying the equation of state to Eq. (17) to eliminate temperature gives:

(18) $$\theta = \frac{\alpha}{R}\frac{(1000\ mb)^{\kappa}}{p^{\kappa-1}}$$

where α is specific volume and R is the universal gas constant.

Taking the logarithm of (18) obtains:

(19) $$\ln\theta = \ln\alpha - \ln R + \kappa\ln(1000\,mb) - (\kappa-1)\ln P.$$

Partially differentiating (19) with respect to time:

(20 a, b) $$\frac{1}{\theta}\frac{\partial\theta}{\partial t} = \frac{1}{\alpha}\frac{\partial\alpha}{\partial t}\ ;\ \frac{1}{\theta}\nabla\theta = \frac{1}{\alpha}\nabla\alpha.$$

Eliminate α from the hydrostatic relation to obtain:

(21 a, b) $$\frac{1}{\theta}\frac{\partial\theta}{\partial t} = \left(-\frac{\partial\pi}{\partial p}\right)^{-1}\frac{\partial}{\partial t}\left(-\frac{\partial\phi}{\partial p}\right)\ ;\ \frac{1}{\theta}\nabla\theta = \left(-\frac{\partial\pi}{\partial p}\right)^{-1}\nabla\left(-\frac{\partial\phi}{\partial p}\right).$$

Division of (16) by and substitution from (21 a, b) is the next step:

(22) $$0 = \left(\frac{\partial\pi}{\partial p}\right)^{-1}\frac{\partial}{\partial t}\frac{\partial\phi}{\partial p} + \underset{\sim}{V}\cdot\nabla\frac{\partial\phi}{\partial p}\left(\frac{\partial\pi}{\partial p}\right)^{-1} + \frac{\omega}{\theta}\left[\frac{\partial\theta}{\partial p} - \frac{\theta L}{c_p T}\left(\frac{dq_w}{dp}\right)_{MA}\right],$$

Multiply by $\partial\pi/\partial p$ to obtain the first law of thermodynamics in terms of the height of a constant pressure surface:

(23) $$\frac{\partial}{\partial t}\left(\frac{\partial\phi}{\partial p}\right) = -\underset{\sim}{V}\cdot\nabla\frac{\partial\phi}{\partial p} - \omega\left[\frac{\partial\ln\theta}{\partial p}\frac{\partial\phi}{\partial p} - \frac{\delta R L}{c_p p}\left(\frac{dq_w}{dp}\right)\right],$$

where $\delta = 1$ for saturation and upward motion, otherwise $\delta = 0$.

The hydrodynamic equation is:

(24) $$\nabla^2 \frac{\partial \Phi}{\partial t} = - f_0 \underset{\sim}{V} \cdot \nabla \eta + f_0^2 \frac{\partial \omega}{\partial p}$$

Taking the horizontal Laplacian of (23) and partially differentiating (24) with respect to pressure and then subtracting to eliminate the local time derivatives, an expression for ω involving moist-adiabatic motion (i. e., a moist ω-equation) is obtained:

(25) $$\left\{ \left[\sigma - \frac{\delta R L}{c_p p} \left(\frac{dq_s}{dp} \right)_{MA} \right] \nabla^2 + f_0^2 \frac{\partial^2}{\partial p^2} \right\} \omega_m = - f_0 \frac{\partial}{\partial p} (-\underset{\sim}{V} \cdot \nabla \eta) + \nabla^2 \left(-\underset{\sim}{V} \cdot \nabla \frac{\partial \Phi}{\partial p} \right).$$

The horizontal Laplacian of the coefficient of ω in Eq. (23) is neglected. It is hoped that this is horizontally linear or nearly so, to prevent the introduction of any ill side effects. For simplicity the following notations are adopted:

(26) a. $$\sigma_0 = \sigma = \frac{\partial \ln \theta}{\partial p} \frac{\partial \Phi}{\partial p},$$

b. $$\sigma_m = \sigma_0 - \frac{\delta R L}{c_p p} \left(\frac{dq_s}{dp} \right)_{MA},$$

c. $$F = - f_0 \frac{\partial}{\partial p} (-\underset{\sim}{V} \cdot \nabla \eta) + \nabla^2 \left(-\underset{\sim}{V} \cdot \nabla \frac{\partial \Phi}{\partial p} \right).$$

Note that $\sigma_0 = 0$ for dry adiabatic lapse rate and $\sigma_m = 0$ for a moist adiabatic lapse rate. Thus, Eqs. (12) and (25) become, respectively:

(27) $$\left[\sigma_0 \nabla^2 + f_0^2 \frac{\partial^2}{\partial p^2} \right] \omega_0 = F,$$

(28) $$\left[\sigma_m \nabla^2 + f_0^2 \frac{\partial^2}{\partial p^2} \right] \omega_m = F$$

The next step is to assume a distribution of ω. A relatively simple and reasonable three-dimensional sinusoidal distribution of ω is assumed. Thus, ω may be represented by:

(29) $$\omega (x, y, p, t) = K \sin \frac{\pi (x - ct)}{A} \sin \frac{\pi (y - ct)}{B} \sin \frac{\pi p}{C},$$

where A, B, and C are wave lengths of the vertical motion field, with the scale being equal to one-half the wavelength.

The following expressions are obtained by operating on Eq. (29):

(30) a. $$\nabla^2\omega = \frac{\partial^2\omega}{\partial x^2} + \frac{\partial^2\omega}{\partial y^2} = -\left[\left(\frac{2\pi}{A}\right)^2 + \left(\frac{2\pi}{B}\right)^2\right]\omega,$$

b. $$\frac{\partial^2\omega}{\partial p^2} = -\left(\frac{2\pi}{C}\right)^2\omega.$$

Substitution of these expressions into Eqs. (27) and (28) leads to:

(31) $$\omega_{0,m} = \frac{-F}{\left(\frac{2\pi f_0}{C}\right)^2\left[1 + \frac{\sigma_{0,m}\left(\frac{1}{A^2}+\frac{1}{B^2}\right)}{(f_0/g)^2}\right]}$$

From this, the desired expression for the ratio of the vertical motions is:

(32) $$\frac{\omega_m}{\omega_0} = \frac{1 + \frac{\sigma_0\left(\frac{1}{A^2}+\frac{1}{B^2}\right)C^2}{f_0^2}}{1 + \frac{\sigma_m\left(\frac{1}{A^2}+\frac{1}{B^2}\right)C^2}{f_0^2}}$$

The enhancement factor, ω_m/ω_0, is thus seen to depend on the vertical and horizontal scale of the vertical motion field and on the "moist" and "dry" stabilities, which depend primarily on $\partial\theta/\partial p$ and $\left(\partial\psi_a/\partial p\right)_{MA}$. The dry stability is given by σ_0, and the moist, by σ_m.

The enhancement factor, Eq. (32), was evaluated assuming C = 2000mb, $f_0 = 10^{-4}$ sec^{-1}, and a moist adiabatic lapse rate for the 1000- to 500-mb layer having a potential temperature of 293°K at the 1000-mb level (i.e., $\sigma_0 = 2.0 \times 10^{-2}$ m^{2}sec^{-2}mb^{-2} and $\sigma_m = 0$). See Table 1 for theoretical enhancement factors, under the above conditions.

Phillips (1963) points out that the quasi-geostrophic approximation is valid for storms having a horizontal scale of 1000km, and larger. This is the usual scale of large-scale precipitation. However in the following

Table 1. Theoretical enhancement factors for a variable horizontal scale and two different values of σ_M.

Vertical Motion Scale(km)	for $\sigma_M = 0$	for $\sigma_M = 0.8 \times 10^{-2}$
2000	2	1.4
1000	5	1.9
500	17	2.3
200	101	2.5
100	401	2.5

work, no such restriction is imposed.

The above enhancement factors should be taken lightly for $\sigma_M = 0$. Ninety atmospheric soundings taken from large-scale precipitation storms show the normal lapse rate in precipitation as less than the moist adiabatic (See Figure 1). This will have an effect on the factors. Table 1 also contains theoretical enhancement factors using a more normal value of $\sigma_M = 0.80 \times 10^{-2} m^2 sec^{-2} mb^{-2}$. The effects of a variable σ_M are demonstrated more clearly in Table 2. At moderate

Table 2. Theoretical enhancement factors for variable σ_M with a constant scale and a value of $\sigma_p = 2.0 \times 10^{-2} m^2 sec^{-2} mb^{-2}$.

σ_M ($\times 10^{-2} m^2 sec^{-2} mb^{-2}$)	(scale=1000km)	(scale=250km)
0.00	5.0	65.0
0.20	3.6	8.8
0.40	2.8	4.7
0.60	2.3	3.2
0.80	1.9	2.4
1.00	1.7	2.0

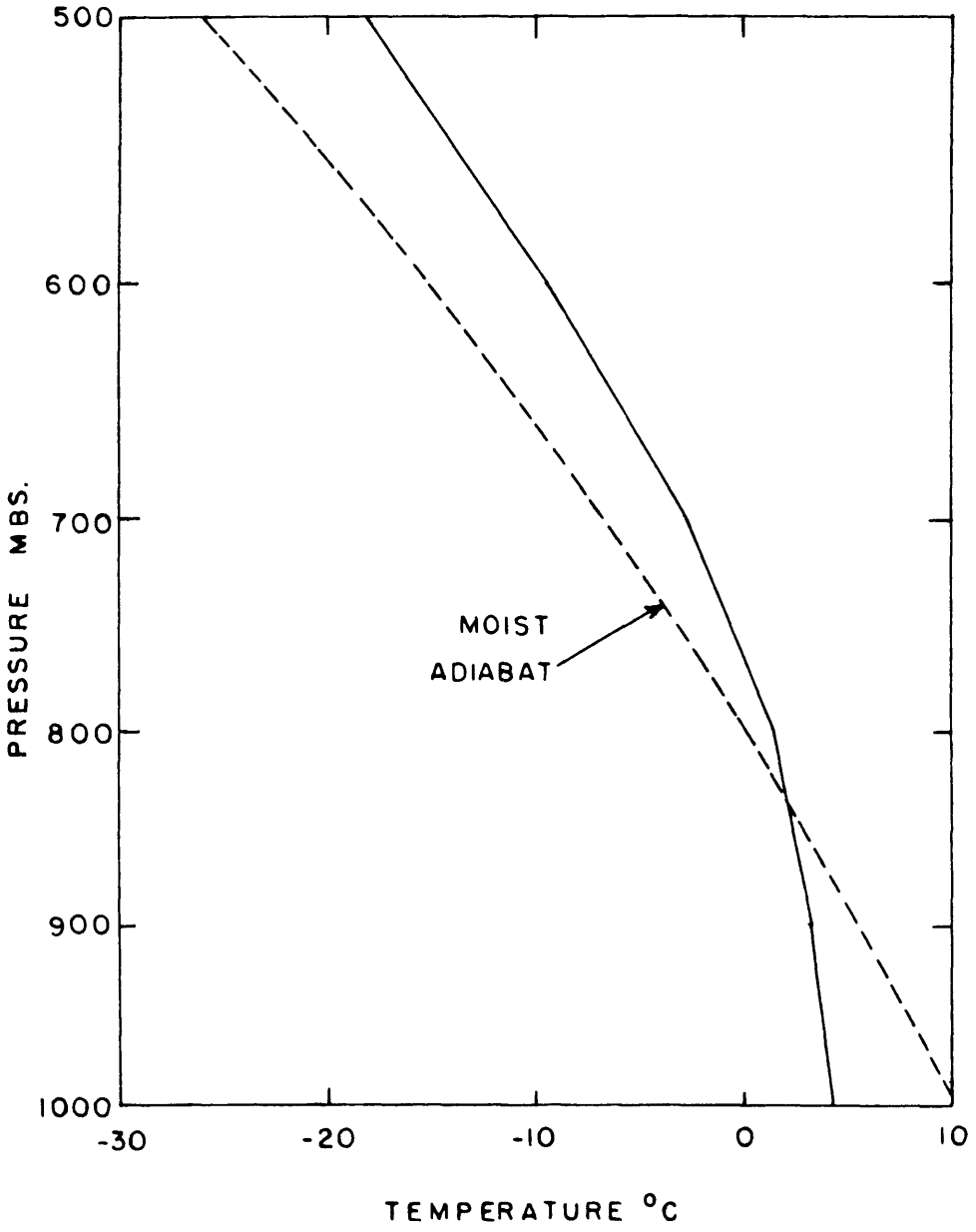

Figure 1. Mean lapse rate of temperature for 90 soundings in large-scale winter precipitation compared to a moist adiabatic lapse rate. Selection was random.

values of σ_M , factors appear relatively insensitive to variations of scale, while at low stability great sensitivity is noted.

In summary an equation for the enhancement factor arising from inclusion of latent heat in the ω -equation has been derived. Assuming a moist adiabatic lapse rate (i.e., $\sigma_M = 0$), theoretical enhancement factors become great as scale decreases. This lapse rate is not observed in the cases selected for study, except for a few isolated cases. further considerations indicate normal winter storms(moderate stability and scale) to have theoretical enhancement factors between 2 and 3. Qualitatively, the effect of a variable σ_0 would decrease the factor at small values of σ_M and increase it for large values. Inclusion of latent heat may have important side effects. For example, the wind and thickness fields may be altered. It is hoped that neglect of the possible side effects is not too crucial.

Changes in liquid water content or in the total storage of the atmosphere and the transport of liquid water by the motions of the atmosphere are potential sources of errors, however, it is not thought that either one of these could contribute very great errors. It is still wise to remember that there are some outside sources of error.

III. TREATMENT OF DATA

In the previous section it was shown that by considering the release of latent heat, a ratio of moist model vertical motion to dry model motion could be formulated. This ratio depends on the horizontal scale and the stability of the storm. To test this formulation, several 24-hour rainstorms are investigated by comparing predicted and observed rainfall to enhancement factors calculated from Eq. (32). The cases to be studied were selected from charts normally available on the national facsimile network. The charts used were the 0000- and 1200-GMT surface and 500-mb charts and the observed 24-hour precipitation chart. Since the SLYH model went into operation in September, 1964, only storms from October 1, 1964 to June 15, 1965 were considered.

The problem is to predict accurate rainfall amounts in heavy large-scale winter storms. Thus, selection of storms was based on significant 24-hour observed amounts and the presence of a continuous area of precipitation. It was also decided to confine cases to the eastern two-thirds of the United States and Canada, reducing orographic effects to a minimum. An attempt was made to confine rainfall to continental areas as much as possible.

The storms selected vary considerably in location and time, covering all sections of the eastern United States and range from December 4, 1964 to April 16, 1965. No cases were selected in

October and June. SLYH saturation deficit predictions were not available for November and May. The cases selected are for 24-hour periods ending at 1200-GMT on the date used to identify the storm. Reference to cases shall be by this date. A list of the cases is contained in LIST OF FIGURES.

The observed precipitation represents a smoothed analysis of 24-hour precipitation data received via facsimile. See Figures 22 to 37 in the Appendix for observed rainfall maps. Systematic errors are unlikely, since the smoothings were random. Work charts were analyzed at intervals sufficiently close to define the field.

To obtain the predicted precipitation, the negative saturation deficits are summed from the two 12-hour SLYH forecasts covering the 24-hour period. The use of 12-hour predictions minimizes possible wind and thickness errors. Values outside the zero isopleth of saturation deficit are treated as zero. The observed thickness halfway through the period is obtained. Table 5 of the Appendix yields precipitation depth for values of thickness and saturation deficit. This is accomplished at each grid point(See Figure5). It would be more desirable to use the SLYH forecast thickness in the Table, but it is not explicitly preserved. Use of the observed thickness is not thought to alter seriously the results.

The assumption of a sinusoidal distribution of ω implies an elliptical precipitation area. Measurement of the scale of the storms

was accomplished by shading the area of precipitation on the 12-hourly surface charts for regular synoptic times and then obtaining a best-fitting (by eye) ellipse to the shaded area. Measurements were made along the axes of the ellipses [A and B in Eq. (32)].

The last data needed before doing the calculations are the moist and dry stabilities. In the derivations of the SLYH and the Reed (1963) models, climatological values of $\partial\theta/\partial p$ are used to evaluate certain coefficients. The net effect of this is the assumption of a constant σ_0. For consistency, a mean value of $\partial\theta/\partial p$ from Petterssen (1956) gave $\sigma_0 = 2.0 \times 10^{-2} m^2 sec^{-2} mb^{-2}$. This is used throughout the following work. The moist stability is to be evaluated from actual atmospheric soundings. All soundings located in actively precipitation areas were plotted (only temperature and humidity curves to 500-mb are needed). Values of σ_m may be calculated for each sounding from Eq. (26 b).

The moist stability should be most representative of the layer contributing the most to the condensation process. To determine this, 20 random soundings were selected. The vertical distribution of condensation was obtained by assuming a sinusoidal vertical motion profile as in Figure 2a and applying Fulks' (1935) graph. Figure 2b is the profile thus obtained. The significant layer is determined to be the 900- to 500-mb layer, although the 800- to 600-mb layer would probably yield similar results.

In calculating σ_m, the mid-point or 700-mb temperature and

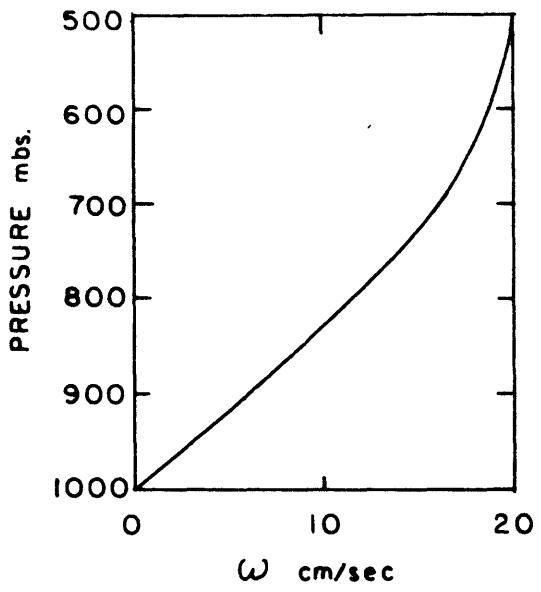

Figure 2a. The assumed vertical velocity profile for = 20 cm sec^{-1} at the 500-mb level.

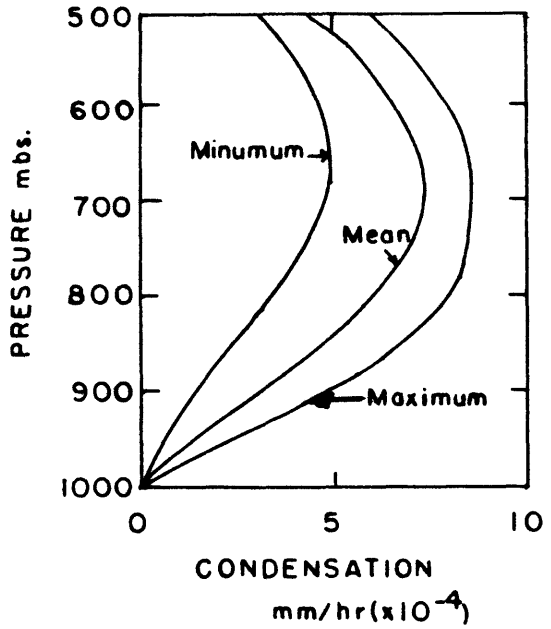

Figure 2b. Resulting mean condensation profile from Fulks' (1935) and Fig. 2a for 20 random soundings.

potential temperature are used and $\partial\theta/\partial p$ and $\left(\partial q_s/\partial p\right)_{MR}$ are replaced by finite-difference approximations. Of approximately 300 values of stability, a very few (10-15) were negative. Normal values of σ_M in precipitation are about $0.8 \times 10^{-2} m^2 sec^{-2} mb^{-2}$. Where frontal inversions extend above the 900-mb level or in very cold air, σ_M is much larger, about 1.5×10^{-2}.

A test was conducted to determine the adequacy of the NMC grid in representing the observed precipitation. In the two cases tested, mean values of precipitation averaged over the area of precipitation were 0.57 and 0.65 inches. The mesh length was reduced by one-half and the corresponding mean values of precipitation were 0.585 and 0.67 inches, respectively. Due to the few points and slight amounts of the March 10 case, it seemed worthwhile to use a mesh length one-quarter that of the basic grid. Small values of mean predicted precipitation in the April storms indicated that a reduction in mesh length would improve the results, thus a mesh length of one-half the basic was adopted.

IV. RESULTS AND DISCUSSION

Mean values of the observed precipitation, $\bar{P}_o$, and the predicted precipitation, $\bar{P}_f$, are obtained by a straight averaging process over all of the points contained in an envelope enclosing both the predicted and observed storm. This procedure essentially involves the total predicted and observed amounts as defined by a grid network. These values and their ratio are summarized in Table 3.

In general, the values of $\bar{P}_f$ are between 0.10 and 0.20 inches. The December 18 case of 0.03 inches is due to a forecast band of extremely light precipitation across the Gulf states, while the rainfall was of much larger extent, and quantity. This case is questioned due to the critical effect that small errors estimating $\bar{P}_f$ have on the ratio. In the case of the other small $\bar{P}_f$, a smaller grid was used, and the entire storm was over land--more confidence was established in the values.

The mean observed precipitation shows more variability and is mostly between 0.20 and 0.50 inches. The unusually low value in the January 8 case is due in large part to a small observed area of rainfall. It also appears to have been a "busted" forecast, so little emphasis shall be placed on the results of this case.

Except for the forementioned cases of December 18 and January 8, the precipitation ratio is consistently in the 2 to 3 range. $\bar{P}_o$ and $\bar{P}_f$ are confidently accurate to about 0.01 to 0.02 inches. This does permit some variation in the ratio due to inaccurate averaging.

Table 3. Results of calculations to determine observed to predicted precipitation ratios and enhancement factors of selected storms.

Case	$\bar{P}_f$ (in.)	$\bar{P}_o$ (in.)	$\frac{P_o}{P_f}$	$\overline{\sigma_m^2}$ ($\times 10^{-2}$) $m^2 sec^{-2} mb^{-2}$	$\frac{\omega_m}{\omega_o}$	$\overline{\sigma_m^2}$ ($\times 10^{-2}$)adj $m^2 sec^{-2} mb^{-2}$	$\left(\frac{\omega_m}{\omega_o}\right)_{adj}$
Dec. 4	0.15	0.50	3.3	0.60	2.94	0.50	3.37
Dec. 11	0.19	0.56	2.9	0.76	2.43	no adjustments	
Dec. 12	0.16	0.30	1.9	0.90	2.12	no adjustments	
Dec. 18	0.03	0.18	6.0	0.68	2.91	0.64	-----
Jan. 8	0.11	0.10	0.9	0.73	2.60	no adjustments	
Jan. 9	0.12	0.30	2.5	0.88	2.25	0.73	2.66
Jan. 23	0.19	0.51	2.7	0.84	2.25	0.70	2.66
Jan. 24	0.19	0.40	2.1	1.25	1.56	1.00	1.91
Feb. 9	0.14	0.29	2.1	0.79	2.36	no adjustments	
Feb. 10	0.19	0.47	2.5	0.84	2.27	0.7[illegible]	2.66
Feb. 25	0.23	0.43	1.9	0.90	2.06	0.80	2.27
Mar. 2	0.15	0.45	3.0	0.72	2.71	0.60	3.17
Mar. 10	0.027	0.071	2.6	0.78	2.53	no adjustments	
Mar. 18	0.14	0.51	3.6	0.78	2.36	0.56	3.15
Apr. 12	0.09	0.27	3.0	0.54	3.39	no adjustments	
Apr. 16	0.10	0.30	3.0	0.68	2.69	no adjustments	

To test the adequacy of the theory, Eq. (32) is applied to the observed scales and mean moist stability, $\overline{\sigma_m}$, to obtain an enhancement factor, or the ratio of the moist and dry vertical motions, ω_m/ω_0. A mean value of σ_m for each case was computed by averaging mean or representative σ_m's for each radiosonde station within the rainfall area. In some instances arbitrary values were assigned to missing stations to eliminate undue bias and any overall non-representativeness.

The enhancement factor equation yields the results listed under in Table 3. Initial notions from the theory attached more importance to the variability of scale than stability. However, in the calculations stability is more important than scale for large-scale, moderate stability winter storms. This is in agreement with final summations of the theory. Situations involving small σ_m are not studied in detail (usually very small in scale), but mention of one such case is made later. The use of precipitation areas to define the field of vertical motion results in an underestimate of ω_m/ω_0, since the vertical motion field may be reasonably assumed to extend slightly beyond the field of precipitation. This is not thought a significant source of error.

Mean values of ω_m/ω_0 for each case are presented for comparison with $\bar{P}_o/\bar{P}_f$. A case by case comparison indicates ω_m/ω_0 to be generally less than $\bar{P}_o/\bar{P}_f$.

During the calculation of σ_m from the plotted soundings many cases

were noted where a frontal surface extended above 900-mbs. These inversions were previously noted to cause an increase in σ_m, due to an increased potential temperature difference, $\Delta\theta$, between 900-mb and 500-mb. Since $\overline{\sigma_m}$ has an effect on ω_m/ω_0, it was decided to check the effects of these inversions. The decrease in $\Delta\theta$ resulting from elimination of the inversion were summed at all stations. A mean "frontal adjustment" for $\Delta\theta$ is put into the first term of σ_m to obtain a "frontal stability adjustment or correction". An adjusted moist stability was then used to determine the final values of . Similar results would have been obtained using the 800- to 600-mb layer or by initially eliminating the inversion.

The net effect of these last computations is to result in a mean $(\omega_m/\omega_0)_{adj}$ for the 16 cases that is closer to the overall precipitation ratio average.

A statistical comparison of $\overline{P}_o/\overline{P}_f$ with the adjusted ω_m/ω_0 was conducted. A correlation coefficient of 0.83 was obtained and a regression equation:

$$\overline{P}_o/\overline{P}_f = (\omega_m/\omega_0)1.39 - 0.92. \tag{33}$$

A plot of ω_m/ω_0 versus $\overline{P}_o/\overline{P}_f$ is presented in Figure 3. The December 18 and January 8 cases were omitted from the statistical comparisons due to their questionable nature. By eye, the regression line does not appear to be significantly different from the ideal dashed regression line. This implies that the regression coefficients should not be significantly

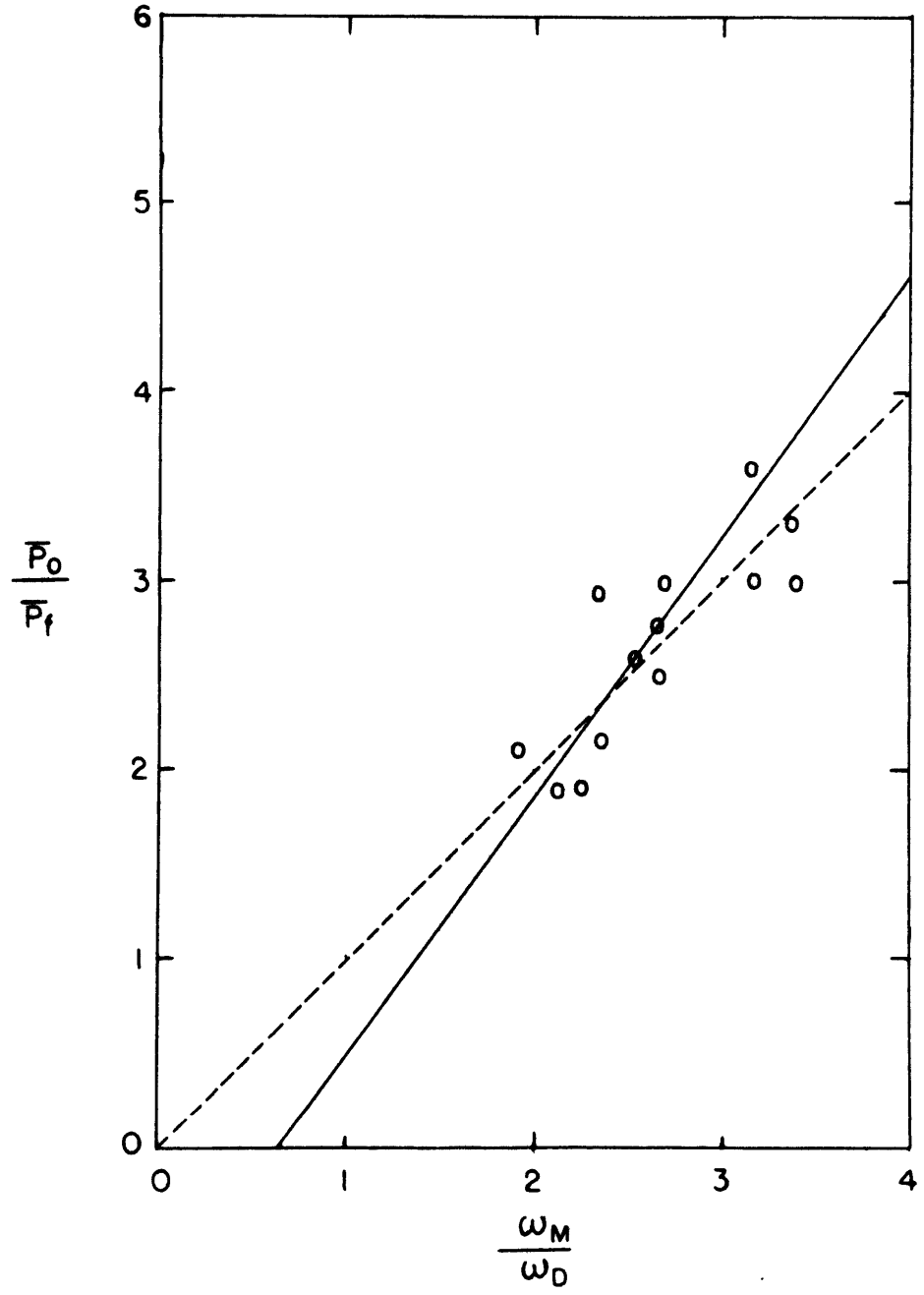

Figure 3. Scatter diagram of theoretical versus observed results. The calculated regression line is solid and the ideal regression line is dashed.

different from 1 and 0, respectively.

The comparison indicates the use of a corrected or adjusted to be suitable for further computations. With the theory justified, the next step is to determine optimum values of ω_M/ω_0 suitable for operational use. Due to the thickness dependence of $\partial\theta/\partial p$ and $\left(\frac{dq_s}{dp}\right)_{MA}$ and thus of σ_M, a similar dependency of ω_M/ω_0 seems appropriate. It is readily adaptable to computer usage, and greater rainfall in southern sections imply a sort of thickness dependence.

The values in Table 4 and in Figure 4 were obtained in a manner similar to previous work. Precipitation means for 60gpm ranges centered on the values in Table 4 were obtained. Values of ω_M/ω_0 were computed, assuming $f_0 = 10^{-4}\text{sec}^{-1}$, C = 2000mb, A = 750km, B = 1500km, and $\sigma_0 = 2.0 \times 10^{-2}\text{m2sec}^{-2}\text{mb}^{-2}$. Adjusted values of σ_M are also used here. Essentially, for each thickness, ω_M/ω_0 is a function of σ_M (adjusted).

At low thicknesses, the $\bar{P}_o/\bar{P}_f$ curve of Figure 4 tends to higher values. For two reasons this is not thought to invalidate the theory. First and most obvious is the few values observed at each thickness in this range. Second and more important is the cold thickness range which could add materially to the observed precipitation in the Great Lakes region through intense low-level convection. This convection would not be predicted by the SLYH model. The values at the other end of the thickness scale appear untrustworthy. As σ_M approaches zero

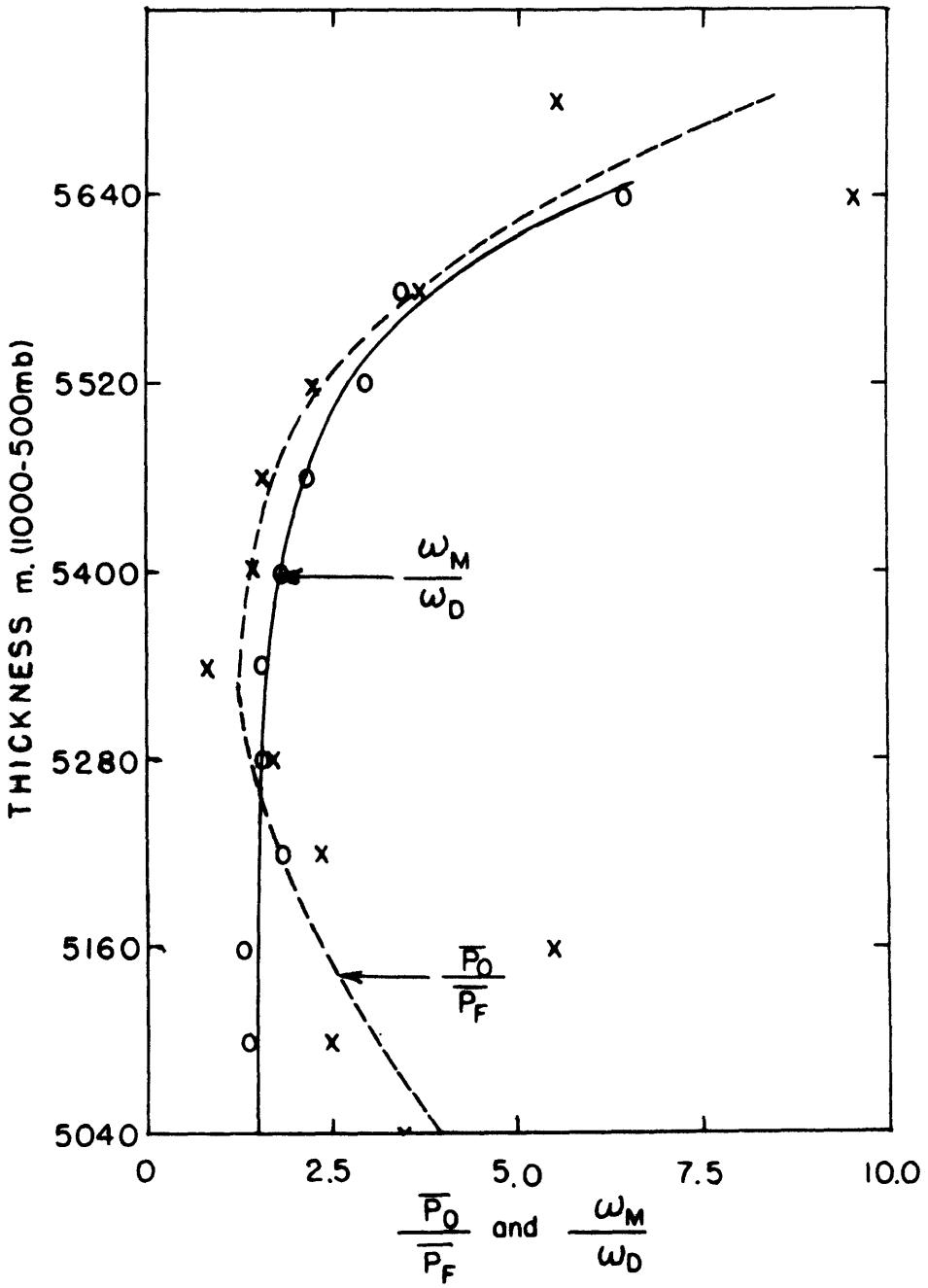

Figure 4. A plot of results of Table 4. The $\overline{P}_o/\overline{P}_f$ curve is a dashed line and the points are x's. The curve is solid and the points are o's.

Table 4. Summary of calculation of $\bar{P}_o/\bar{P}_f$ and ω_m/ω_o on a thickness dependency. Thickness values are the midpoint of a 60-gpm range. Refer also to Figure 4.

Thickness (gpm)	$\bar{P}_f$ (in.)	$\bar{P}_o$ (in.)	$\frac{P_o}{P_f}$	$\overline{\sigma_m}$ (adj)x10^{-2} $m^2 sec^{-2} mb^{-2}$	$\frac{\omega_m}{\omega_o}$
5040	0.02	0.07	3.5	-----	-----
5100	0.06	0.15	2.5	1.45	1.4
5160	0.02	0.11	5.5	1.56	1.3
5220	0.08	0.19	2.3	1.05	1.8
5280	0.07	0.12	1.7	1.22	1.6
5340	0.15	0.13	0.9	1.22	1.6
5400	0.17	0.24	1.4	1.09	1.8
5460	0.21	0.33	1.6	0.87	2.15
5520	0.22	0.49	2.2	0.63	2.9
5580	0.16	0.59	3.7	0.51	3.4
5640	0.08	0.76	9.5	0.22	6.4
5700	0.04	0.21	5.2	-----	------

and the scale becomes small, ω_m/ω_o becomes extremely sensitive to changes of σ_m and scale. There is a tendency for these conditions to occur at higher thicknesses, since the scale seems to become smaller as the stability decreases. Thus, the values of $\bar{P}_o/\bar{P}_f$ at either end of the thickness range are questionable. However, they do indicate a trend.

Noteworthy about the ω_m/ω_o curve in Figure 4 is its relative flatness at about 1.5 through the low and middle thickness range. Aubert(1957) noted a 43% increase of total precipitation due to release of latent heat.

His findings are supported by this portion of the curve. At warmer thicknesses the increase in ω_m/ω_0 is due to larger values of $\left(\frac{dq_w}{dp}\right)_{MA}$ and smaller values of $\partial\theta/\partial p$.

To illustrate this effect on ω_m/ω_0 as σ_m becomes small, consider the case of January 23. This has a small center of heavy precipitation over southern Alabama and Mississippi, with a mean of 2.5 to 3.0 in. and a maximum of 6.8 in. Over this same area $\bar{P}_f$ is close to 0.10 in. Scale is about 200 by 300 km. If a value of $\sigma_m = 0.00$ is assumed (and it is reasonable), a value of $\omega_m/\omega_0 = 56.4$ is obtained. A value of $\sigma_m = 0.10 m^2 sec^{-2} mb^{-2}$ (also reasonable) obtains $\omega_m/\omega_0 = 8.7$. From data presented, $\bar{P}_o/\bar{P}_f$ is approximately 25 to 30. Although inconclusive this seems to indicate, at least, that the theory does not "blow up" at small scale and stability.

Some general observations about the areal distribution of precipitation were noted. As one looks downstream the predicted center of maximum precipitation is located to the left and downstream from the observed maximum. The cause of this appears to be a combination of placing the predicted precipitation at the end of the trajectories and the influence of thickness on ω_m/ω_0 in that thickness range(moderatly high) which would normally be expected over heavy precipitation. The areas tend to have a character similar to the observed precipitation. Excessive observed to predicted precipitation is noted along the Gulf coastal states under the influence of southerly flow. This is very likely partially attributable to

the assumption of a uniform low relative humidity over oceanic regions.

Mean precipitation over the observed areas were not determined, but in general it does not appear to exceed the 2 cm day^{-1} that is permissable by geostrophic approximation, Phillips (1963). The maximum precipitation appears to approach or slightly exceed this figure if it were to be subject to an appropriate averaging process.

Strong frontal inversions above 800-mb were not observed. Many inversions below this level appeared to be losing their character and identity from a cursory survey of the plotted soundings. This suggests that precipitation-producing fronts may be "self-destructive" through the processes of vertical motion, release of latent heat, and condensation. Heavy precipitation-producing fronts thus seem to be shallow. These observations are consistent with the findings of Staley(1965), who finds a tendency for high-moisture inversions to be eroded by radiative cooling.

V. CONCLUSIONS

From the results presented in Table 4 and Figure 4, it is recommended that the enhancement factors, ω_M/ω_0 be adopted on a thickness dependency basis for use with SLYH model predictions. These results have a firm theoretical foundation and are well supported by the precipitation ratios. On the lower end of the thickness scale, it seems advisable to consider the situation more thoroughly. If this truly represents a Great Lakes effect as previously suggested, the $\bar{P}_0/\bar{P}_f$ curve may well be the more accurate.

Before any definite conclusions can be drawn concerning the high end of the thickness scale, more cases are needed to work on the problem of low stability and small scale. It is concluded that the large-scale winter precipitation is capable of being adequately forecast with inclusion of the latent heat effect. For the case of moderate stability, typical of winter precipitation, and relatively large scale, the effects of variability of scale are not important.

The variability of stability and its correlation with precipitation indicate the ultimate desirability of using an explicit moist stability within the prediction model. For the present, a prediction of the moist stability should be useful in precipitation predictions. If this could not be accomplished rigorously, then perhaps estimates could be made, since σ_M does not seem to vary rapidly with time. From Table 4, σ_M is observed to resemble a linear variation with thickness

Thus the neglect of the horizontal Laplacian of σ_M in the derivation appears to be validated.

Previous assumptions of a moist-adiabatic lapse rate in large-scale precipitation are strongly questioned. As shown by Figure 1, 90 random soundings display a smaller lapse rate.

Some tentative conclusions(tentative by number of cases involved) can be drawn concerning the effects of cumulus, fronts and orography on the total precipitation. Recall from the regression Eq. (33) that the coefficients do not appear too different from one and zero, respectively. This indicates that the total precipitation of a storm is not increased by convection, fronts, and orographical features, but that these features only act to redistribute the precipitation. This is in general agreement with the assumptions concerning the transport of liquid water horizontally and that the atmosphere acts as neither a sink nor a source for moisture.

BIBLIOGRAPHY

Aubert, E. F., 1957: On the release of latent heat as a factor in large-scale atmospheric motions. J. Meteor., 14, 527-542.

Collins, G. O., and P. M. Kuhn, 1954: A generalized study of precipitation forecasting, Part 3. Mon. Wea. Rev., 82, 173-182.

Danard, M. B., 1964: On the influence of released latent heat on cyclone development. J. App. Meteor., 3, 27-37.

Estoque, M. A., 1957: An approach to quantitative precipitation forecasting. J. Meteor., 14, 50-54.

Fulks, J. R., 1935: Rate of precipitation from adiabatically ascending air. Mon. Wea. Rev., 63, 291-294.

Kuhn, P. M., 1953: A generalized study of precipitation forecasting, Part 2. Mon. Wea. Rev., 81, 222-232.

Petterssen, S., 1956: Weather Forecasting and Analysis, New York, McGraw Hill, p109.

Phillips, N. A., 1963: Geostrophic motion. Rev. of Geophysics, 1, 123-176.

Reed, R. J., 1963: Experiments in 1000-mb prognosis. Washington, D. C., U. S. Weather Bureau National Meteorological Center Technical Memorandum No. 26, 1-31.

Sanders, F., 1958: Cloudiness and precipitation in relation to large-scale vertical motion and moisture. Cambridge, Mass., Massachusetts Institute of Technology, Dept. of Meteorology, Scientific Report No. 4, 1-30, Contract No. AF19(604)-1305.

Sanders, F., 1963: A prediction model for integrated water vapor, cloudiness and precipitation. in Final Report Contract No. AF19(604)-8373, Dept. of Meteorology, M. I. T. , Cambridge, Mass.

Smagorinsky, J., 1956: On the inclusion of moist adiabatic processes in numerical prediction models. Ber. d. deutsches Wetterd., 5, No. 38, 82-90.

Smagorinsky, J., and G. O. Collins, 1955: On the numerical prediction of precipitation. Mon. Wea. Rev., 83, 53-57.

Smebye, S. J., 1958: Computation of precipitation from large-scale motion. J. Meteor., 15, 547-560.

Spar, J., 1953: A suggested technique for quantitative precipitation forecasting. Mon. Wea. Rev., 81, 217-221.

Staff Members, Tokyo University, 1955: The quantitative forecast of precipitation with the numerical method. J. Meteor. Soc. Japan, 33, 204-216.

Staley, D. O., 1965: Radiative cooling in the vicinity of inversions and the tropopause. Q. J. R. M. S., 91, 282-301.

Swayne, W. W., 1956: Quantitative analysis and forecasting of winter rainfall patterns. Mon. Wea. Rev., 84, 53-65.

Thompson, J. C., and G. O. Collins, 1953: A generalized study of precipitation forecasting, Part 1. Mon. Wea. Rev., 81, 91-100.

Vederman, J., 1961: Forecasting precipitation with the aid of a high-speed electronic computer. Mon. Wea. Rev., 89, 243-250.

Younkin, R. J., J. A. LaRue, and F. Sanders, 1965: The objective prediction of clouds and precipitation using vertically integrated moisture and adiabatic vertical motions, J. App. Meteor., 4, 3-17.

APPENDIX

Table 5.[4] Thickness (h) and precipitation depth (D) per 60-gpm. of negative saturation deficit ($-h_d$). Precipitation amount is the net slope of precipitable water content curve over a 60-gpm. interval (30-gpm below to 30-gpm above the designated thickness value) adjusted to obtain conveniently usable values.

h gpm	D inches	h gpm	D inches
4740	0.01	5340	0.10
4800	0.02	5400	0.12
4860	0.02	5460	0.14
4920	0.03	5520	0.16
4980	0.03	5580	0.18
5040	0.04	5640	0.20
5100	0.04	5700	0.22
5160	0.05	5760	0.25
5220	0.06	5820	0.30
5280	0.08	5880	0.35

[4] From Younkin, LaRue, and Sanders (1965).

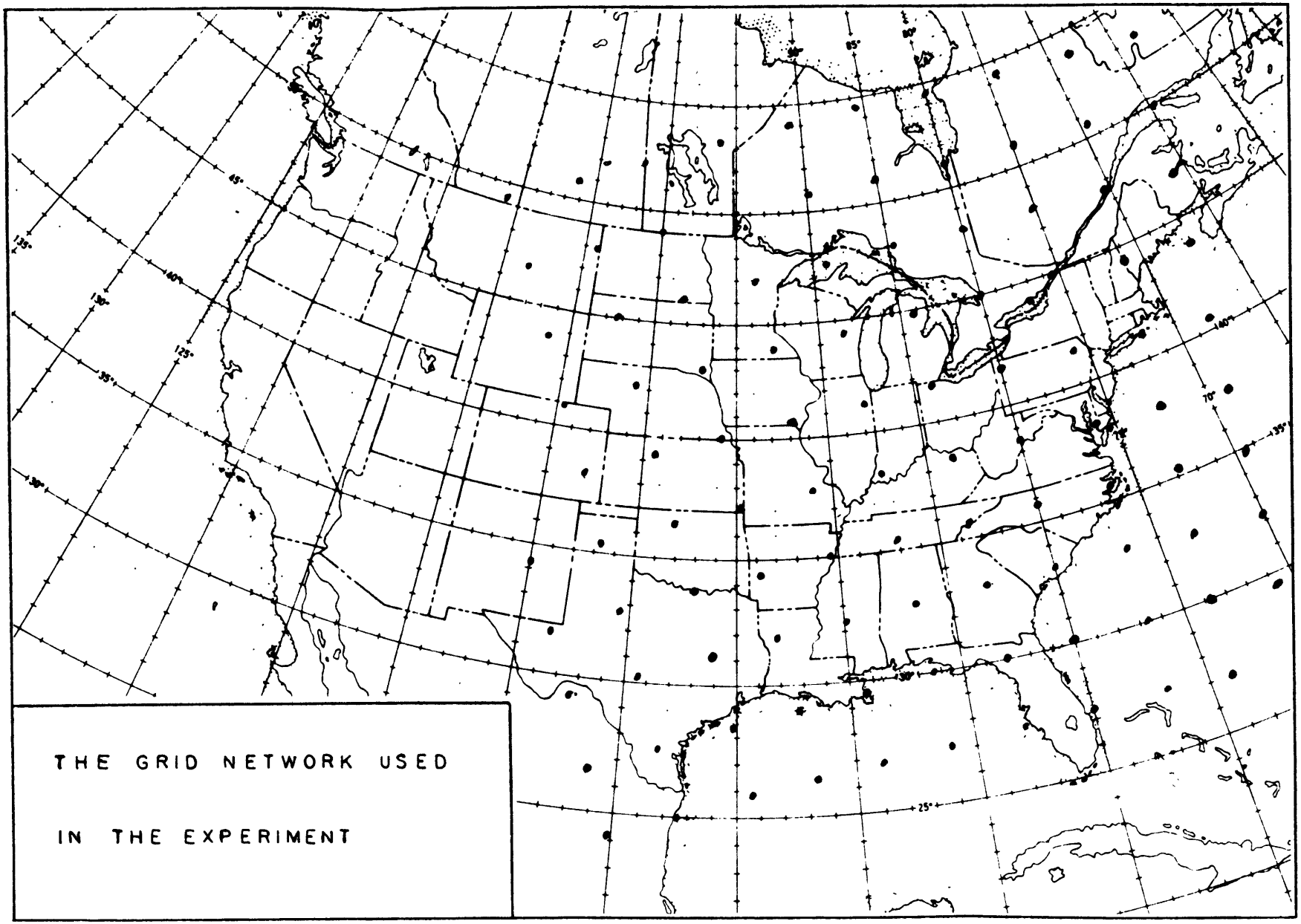

FIGURE 5

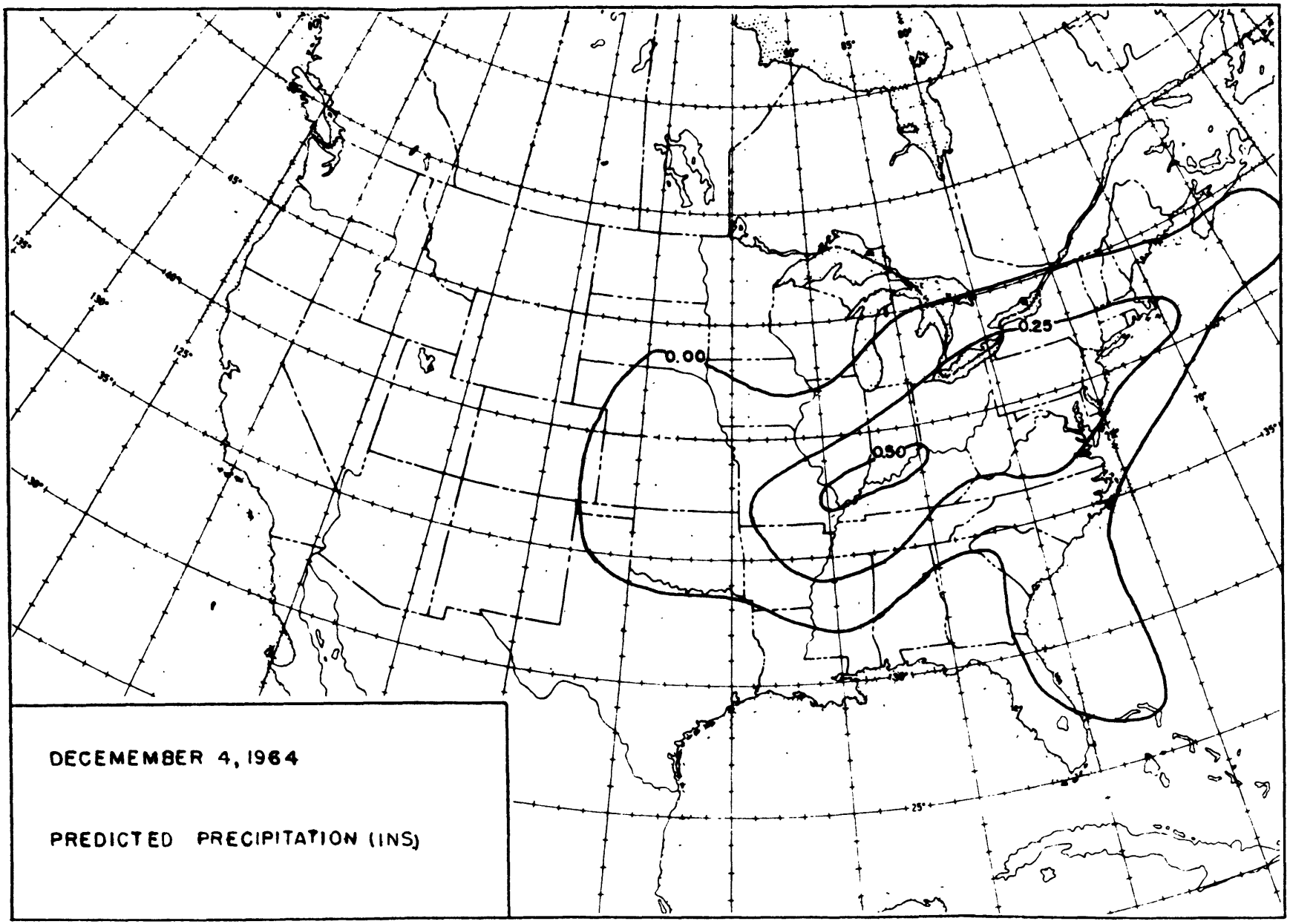

FIGURE 6

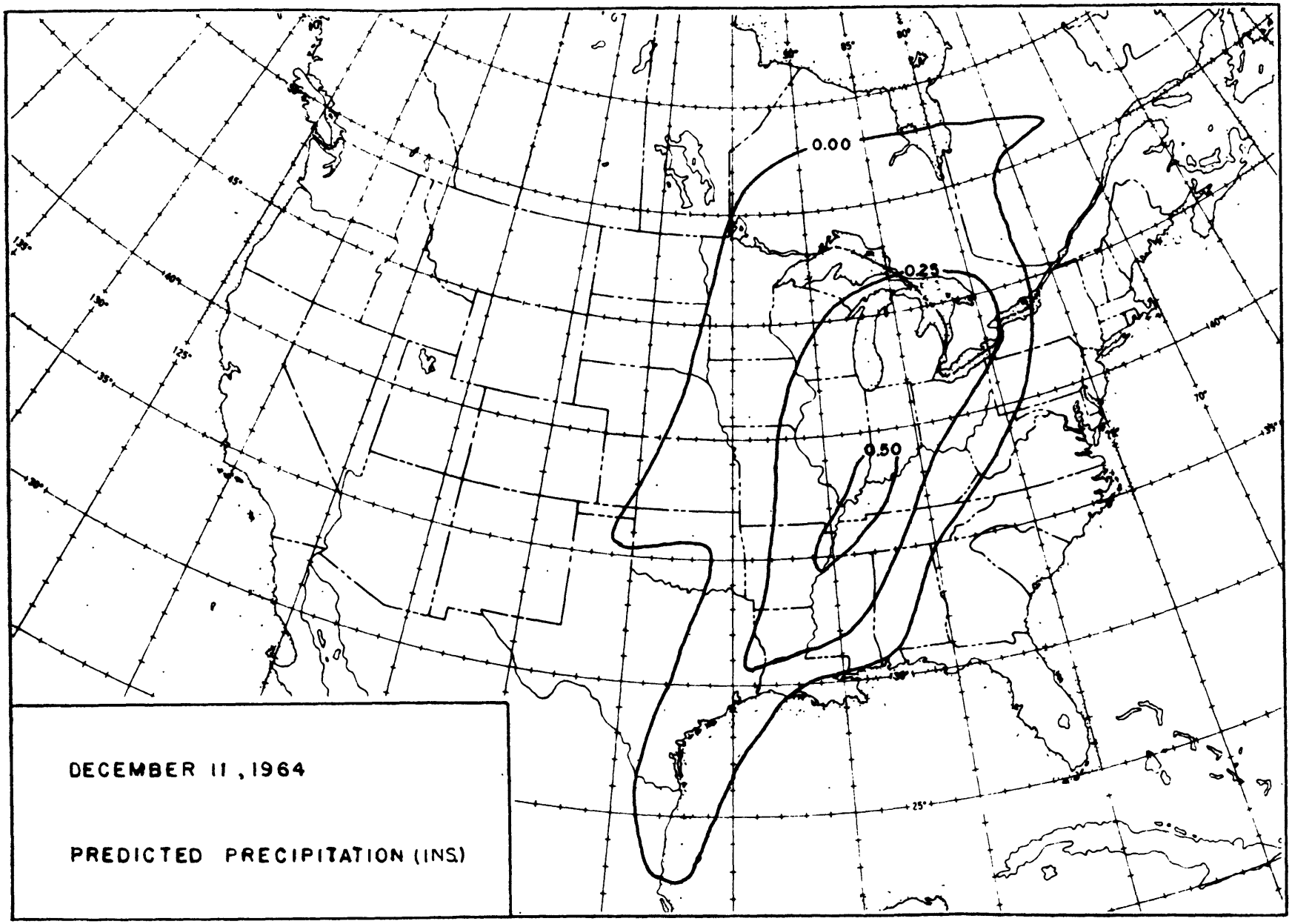

FIGURE 7

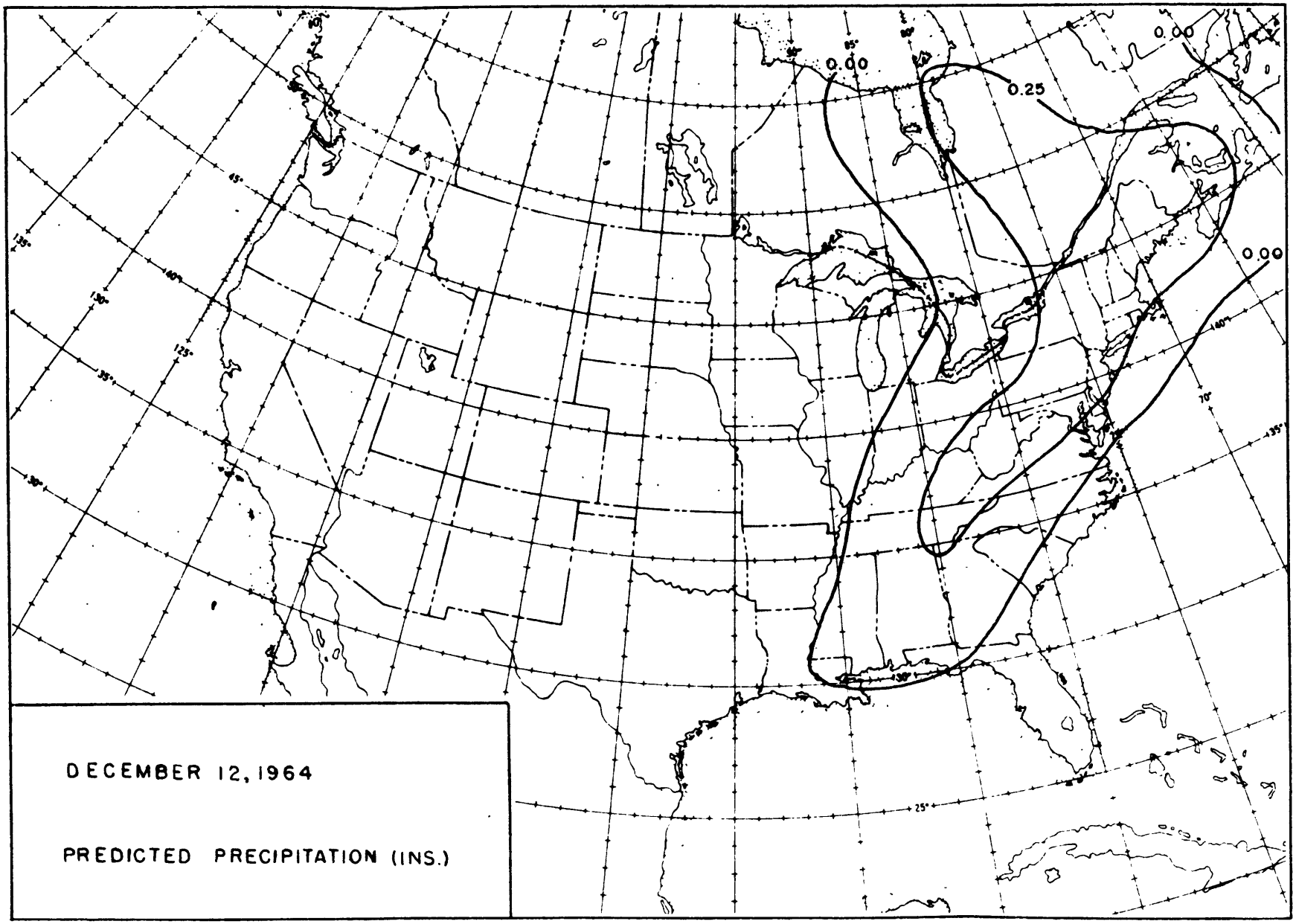
0.00
0.00
0.25
0.00
DECEMBER 12, 1964
PREDICTED PRECIPITATION (INS.)

FIGURE 8

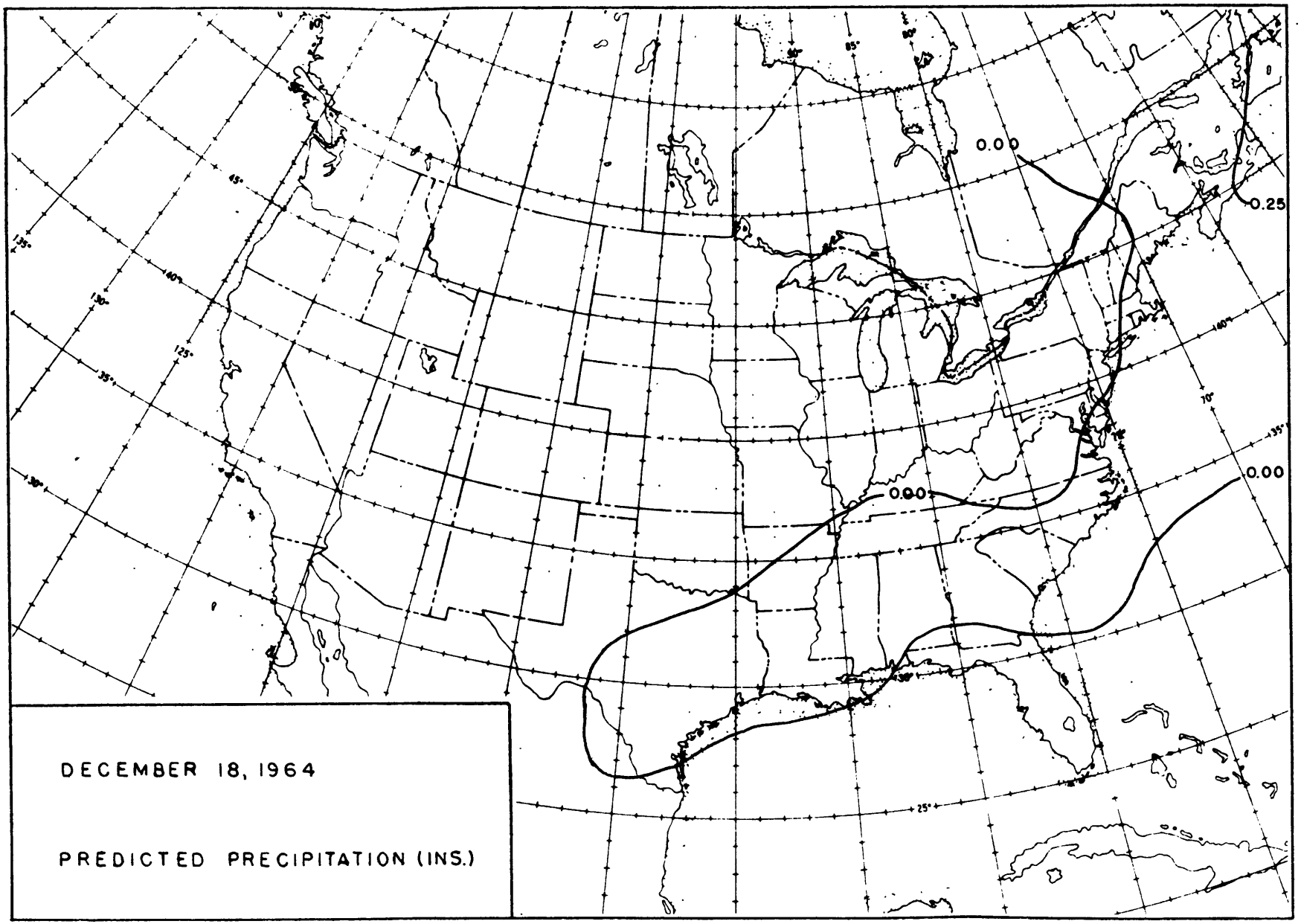
0.00
0.25
0.00
0.00
DECEMBER 18, 1964
PREDICTED PRECIPITATION (INS.)

FIGURE 9

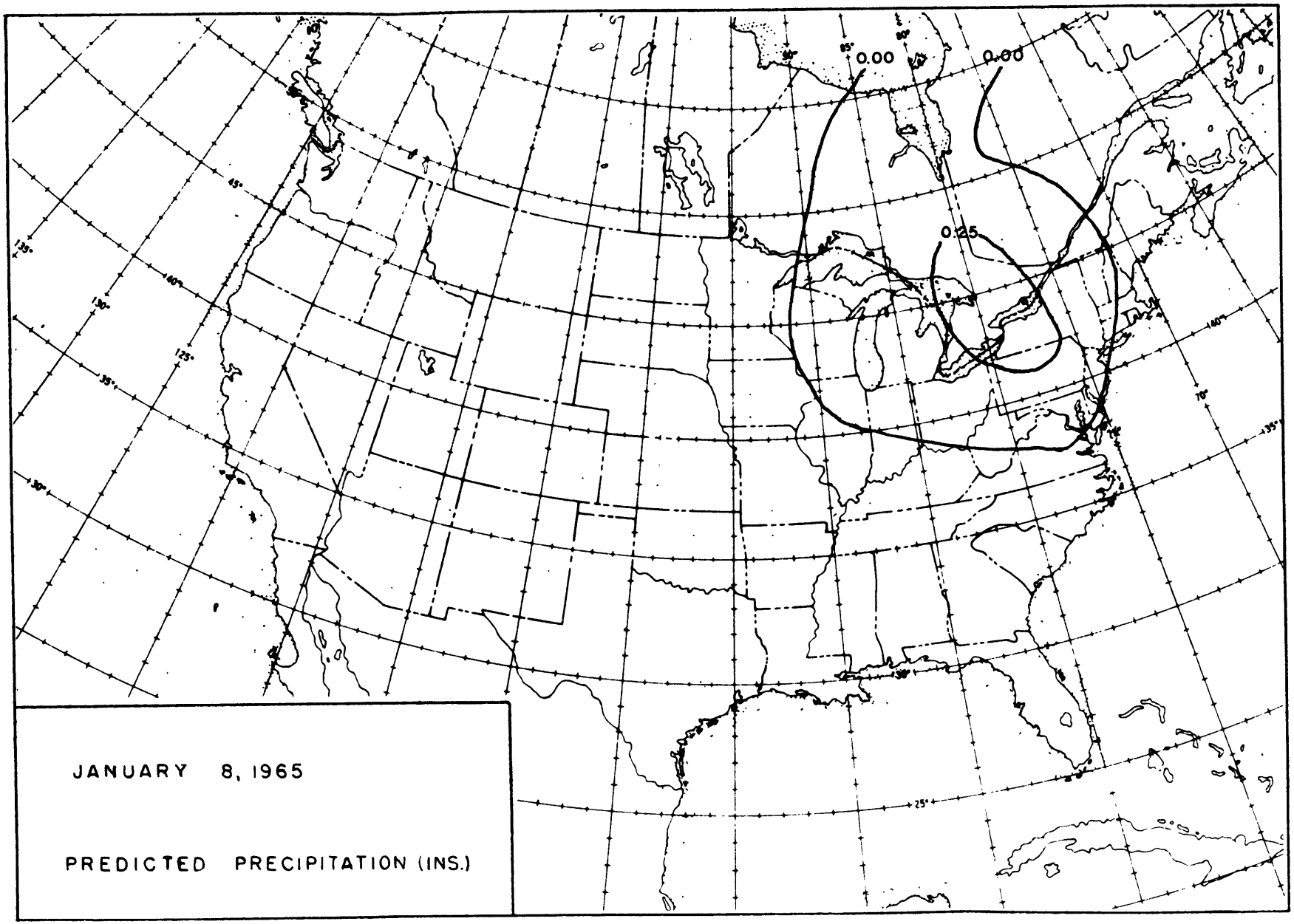

FIGURE 10

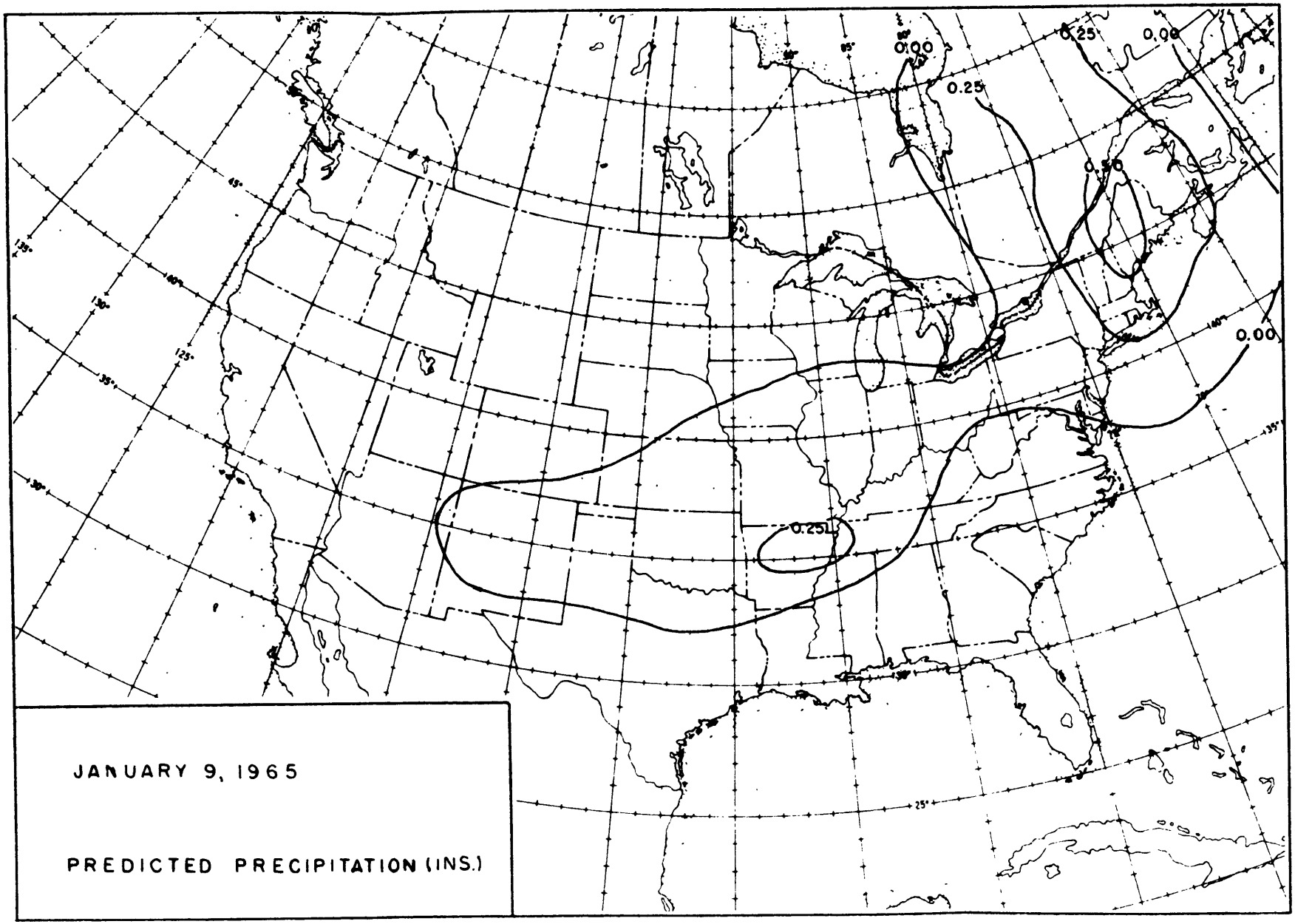
0.00
0.25
0.00
0.25
0.00
0.25
JANUARY 9, 1965
PREDICTED PRECIPITATION (INS.)

FIGURE II

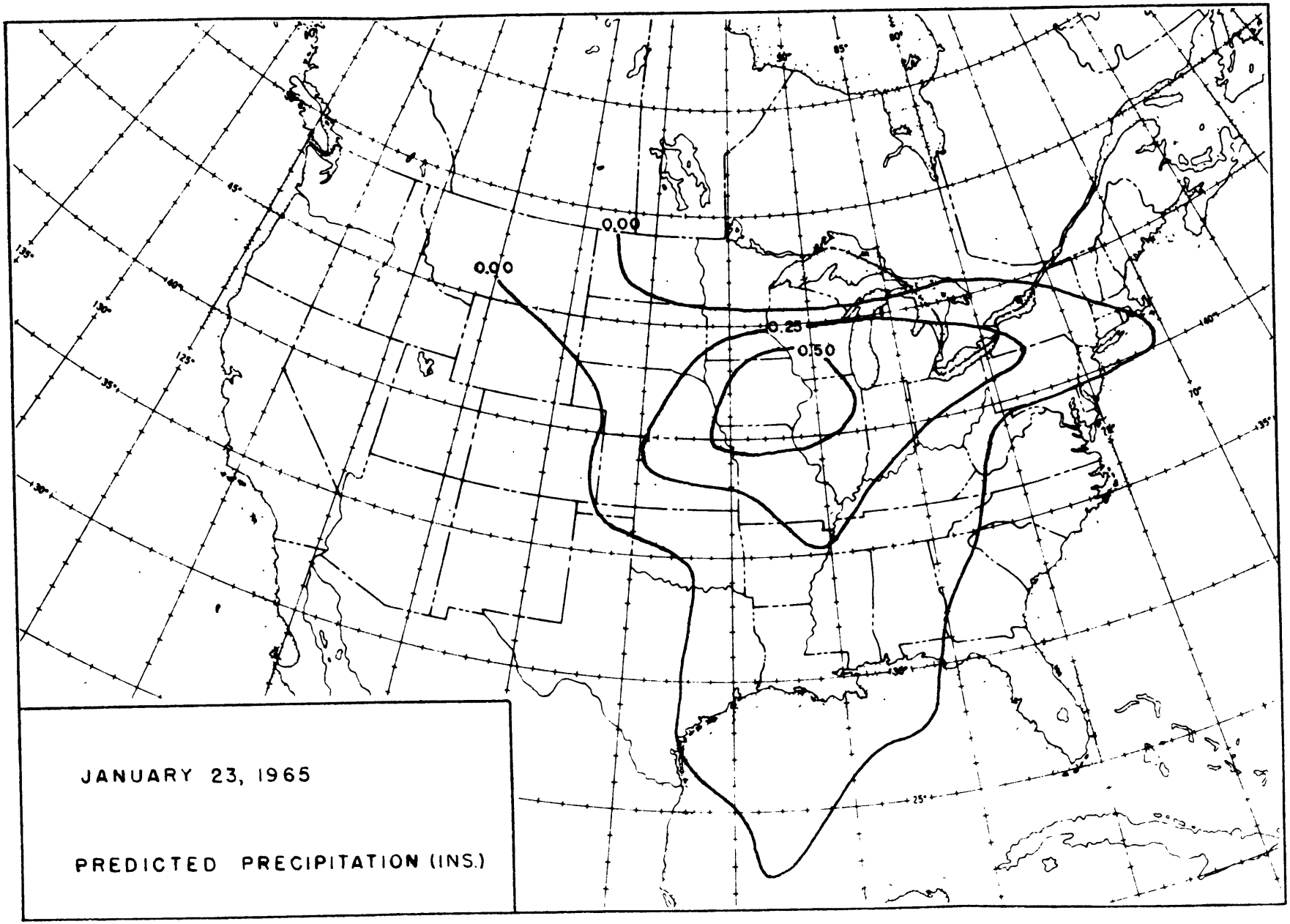
0.00
0.00
0.25
0.50
JANUARY 23, 1965
PREDICTED PRECIPITATION (INS.)

FIGURE 12

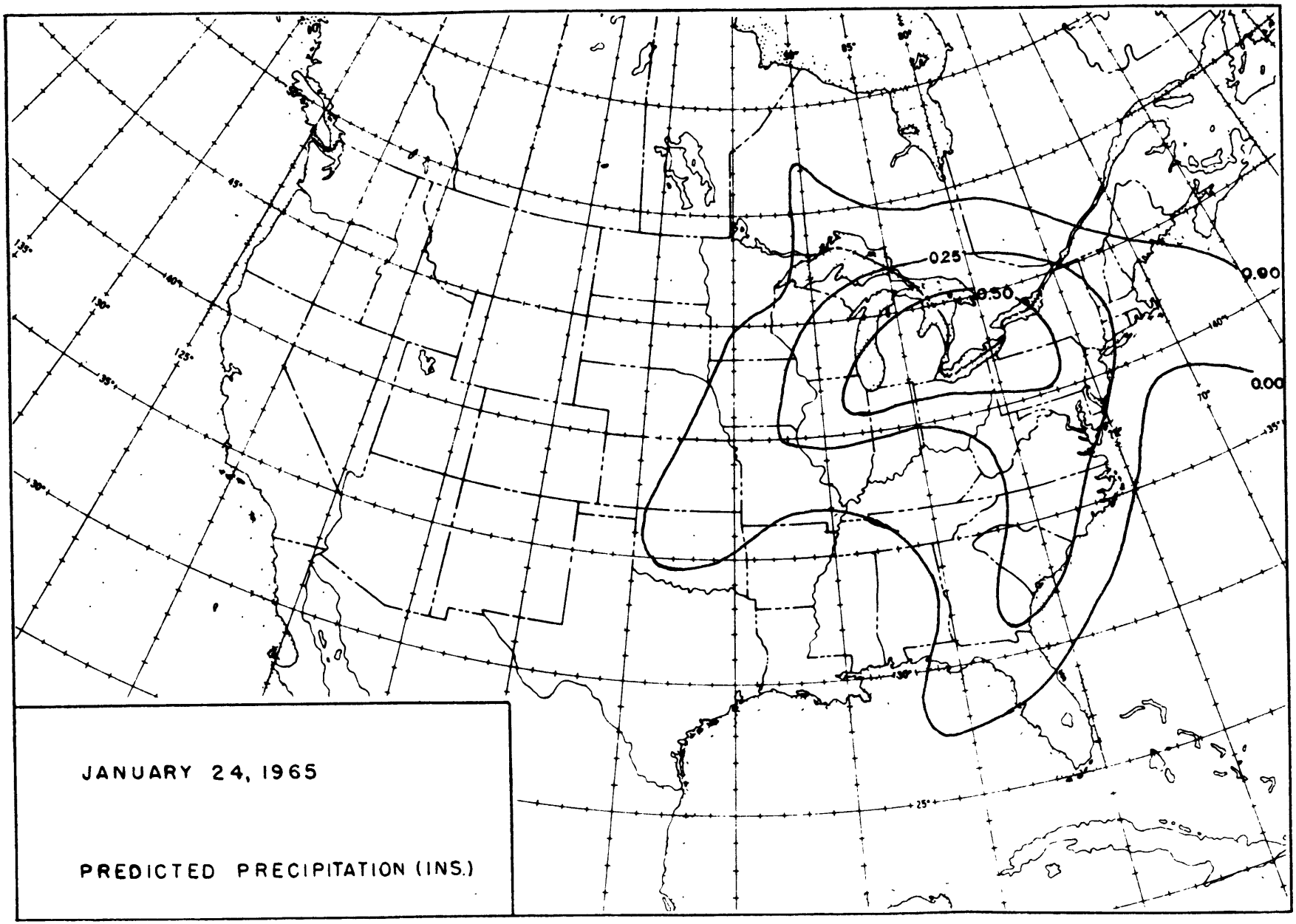
0.25
0.50
0.00
0.00
JANUARY 24, 1965
PREDICTED PRECIPITATION (INS.)

FIGURE 13

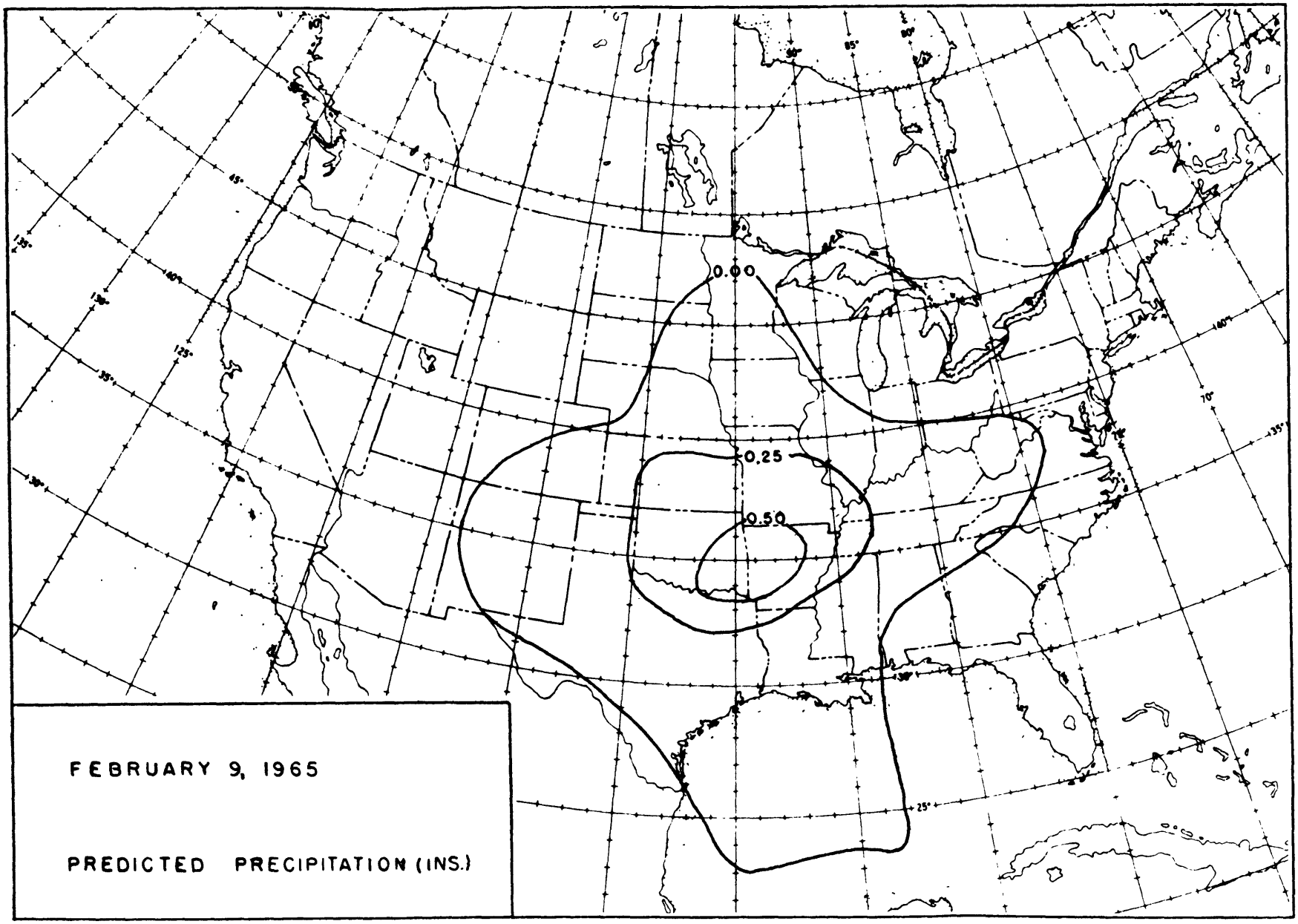

FIGURE 14

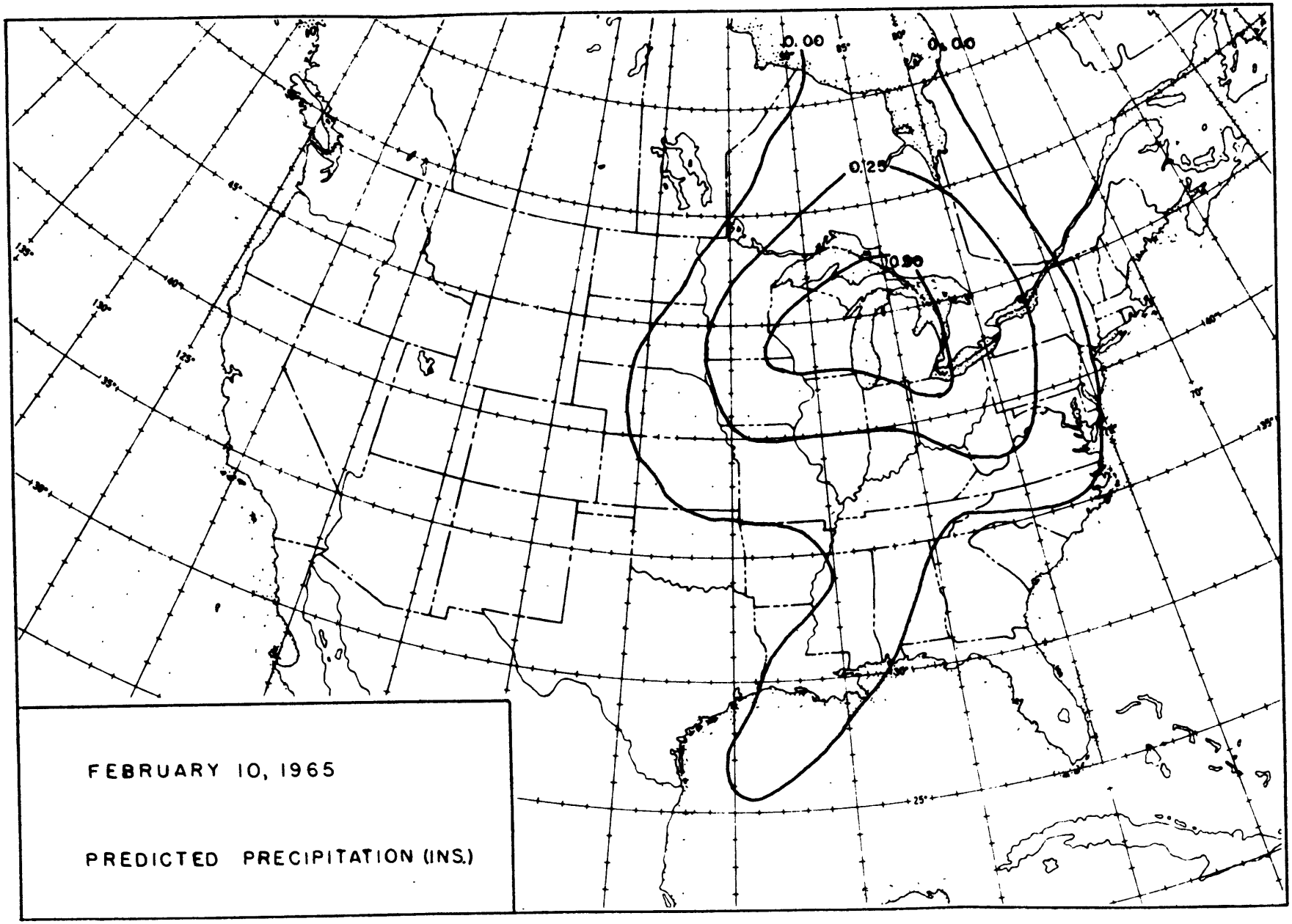
0.00
0.00
0.25
0.50
FEBRUARY 10, 1965
PREDICTED PRECIPITATION (INS.)

FIGURE 15

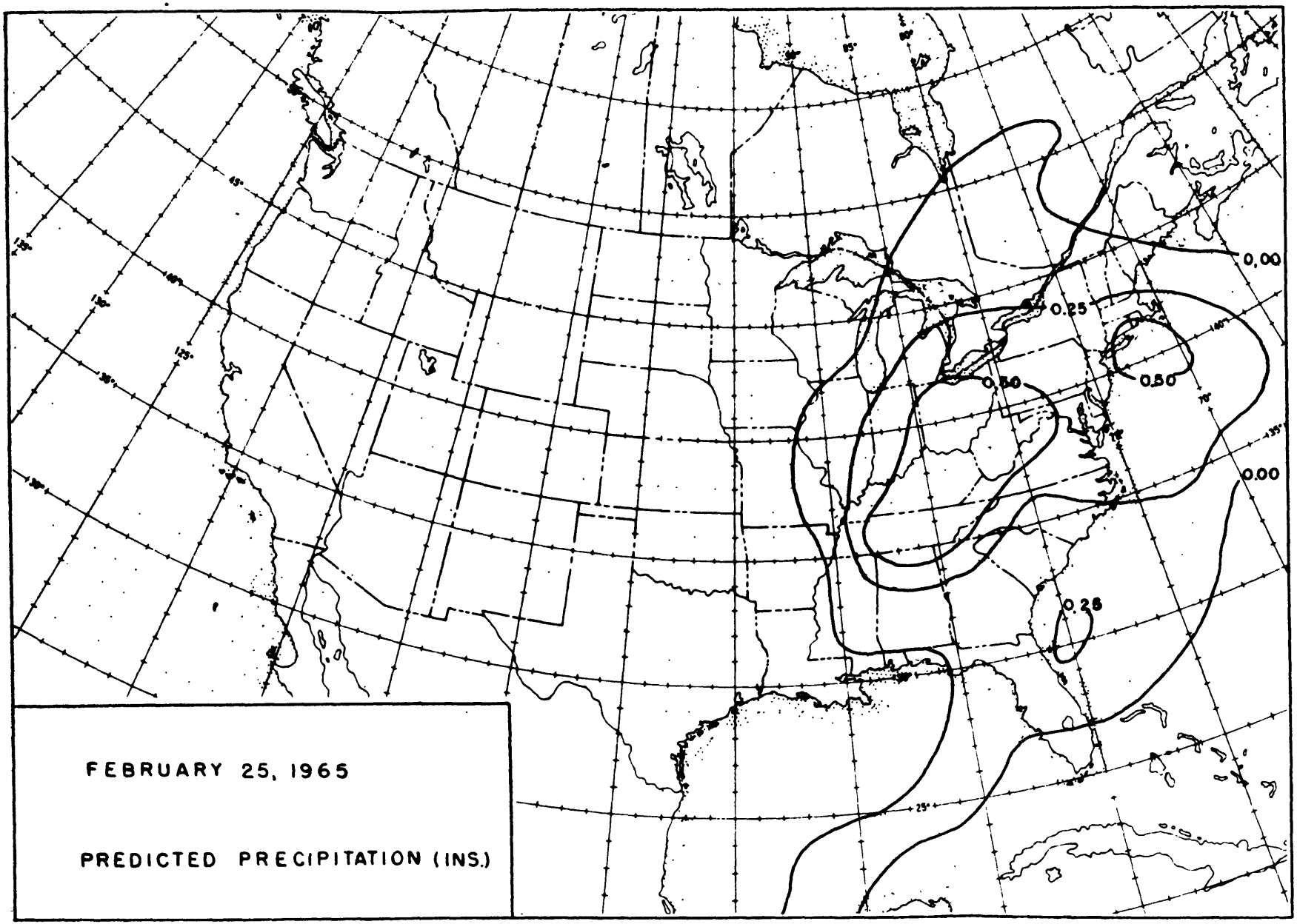
0.00
0.25
0.50
0.50
0.00
0.25
FEBRUARY 25, 1965
PREDICTED PRECIPITATION (INS.)

FIGURE 16

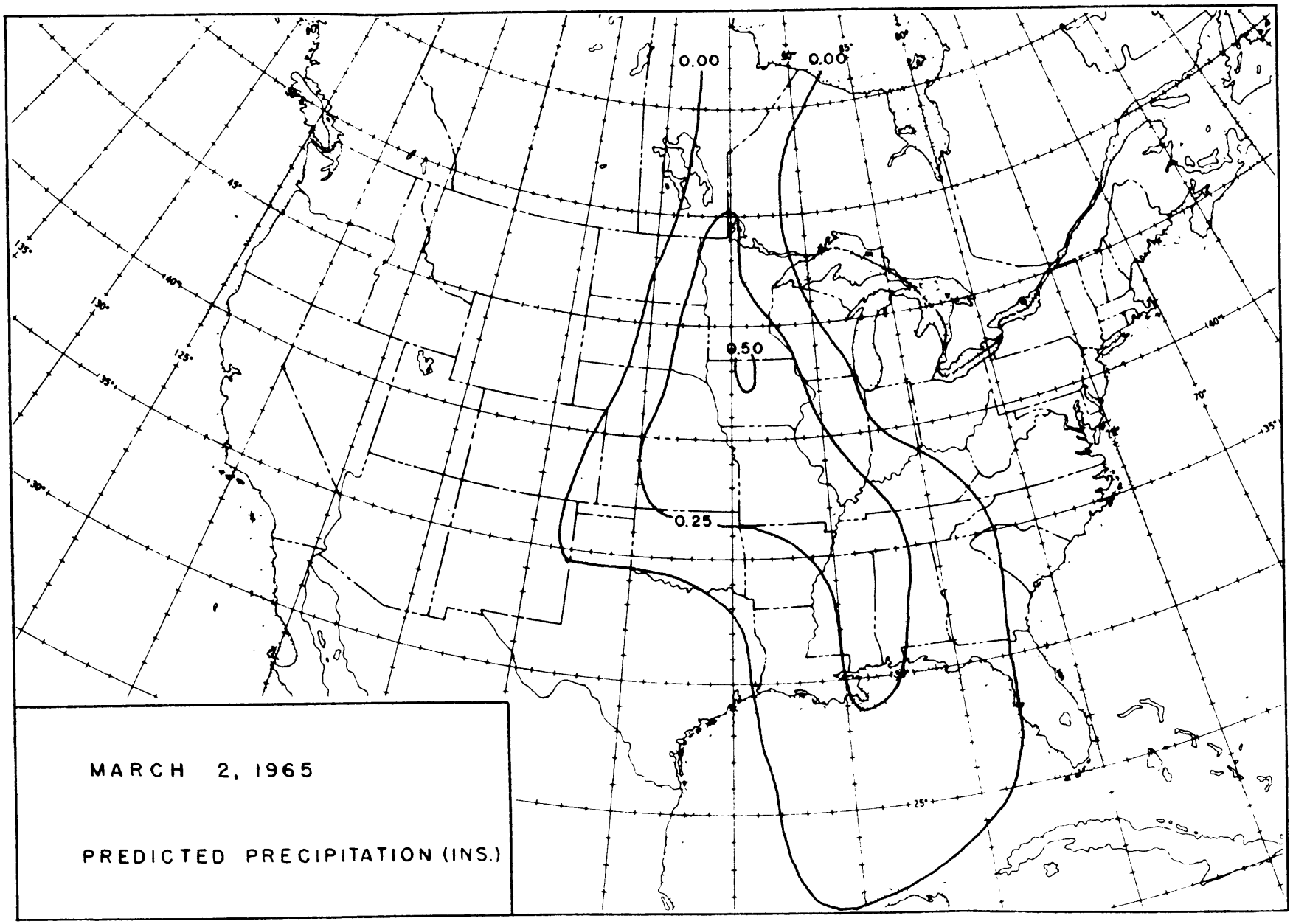

FIGURE 17

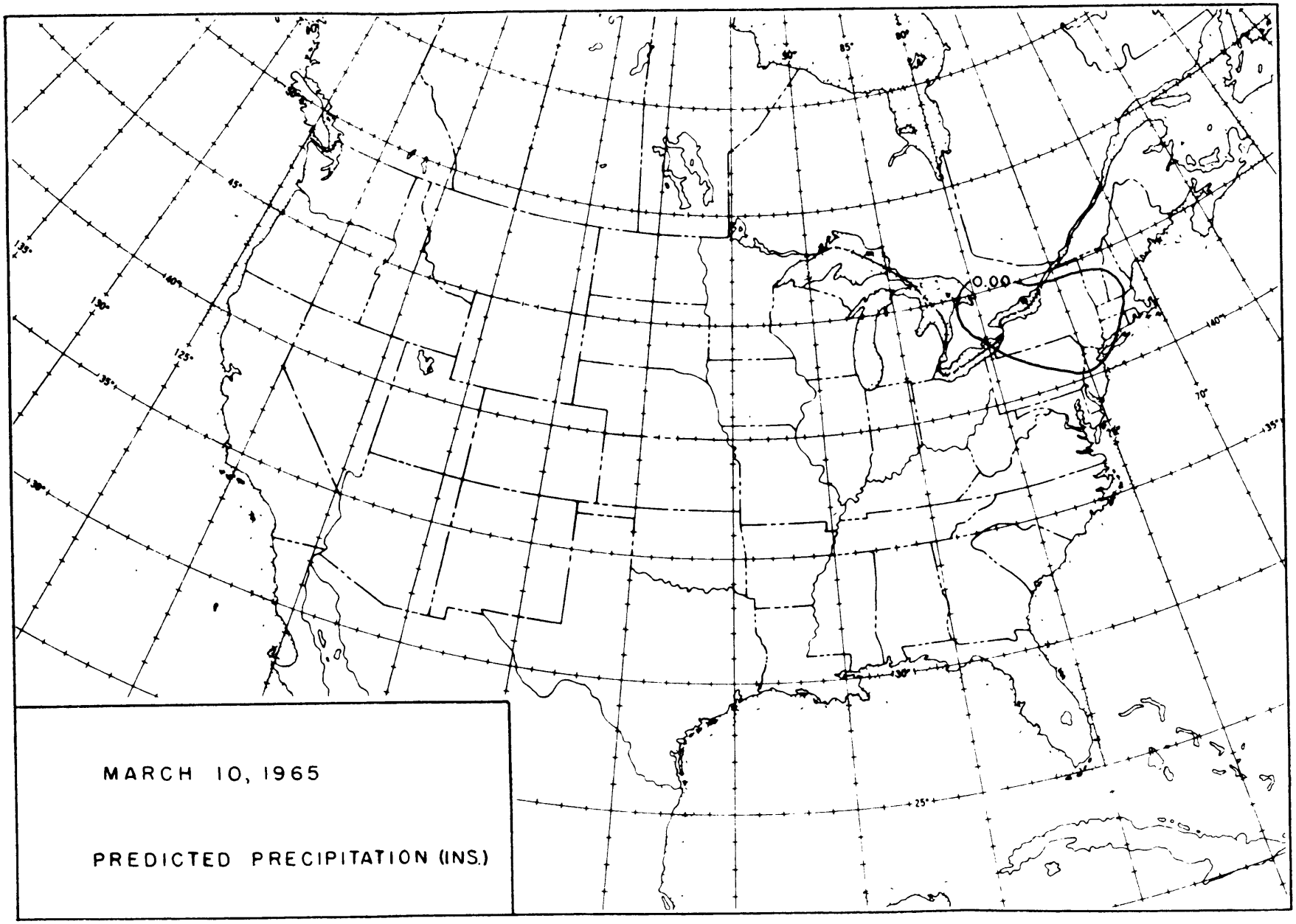

FIGURE 18

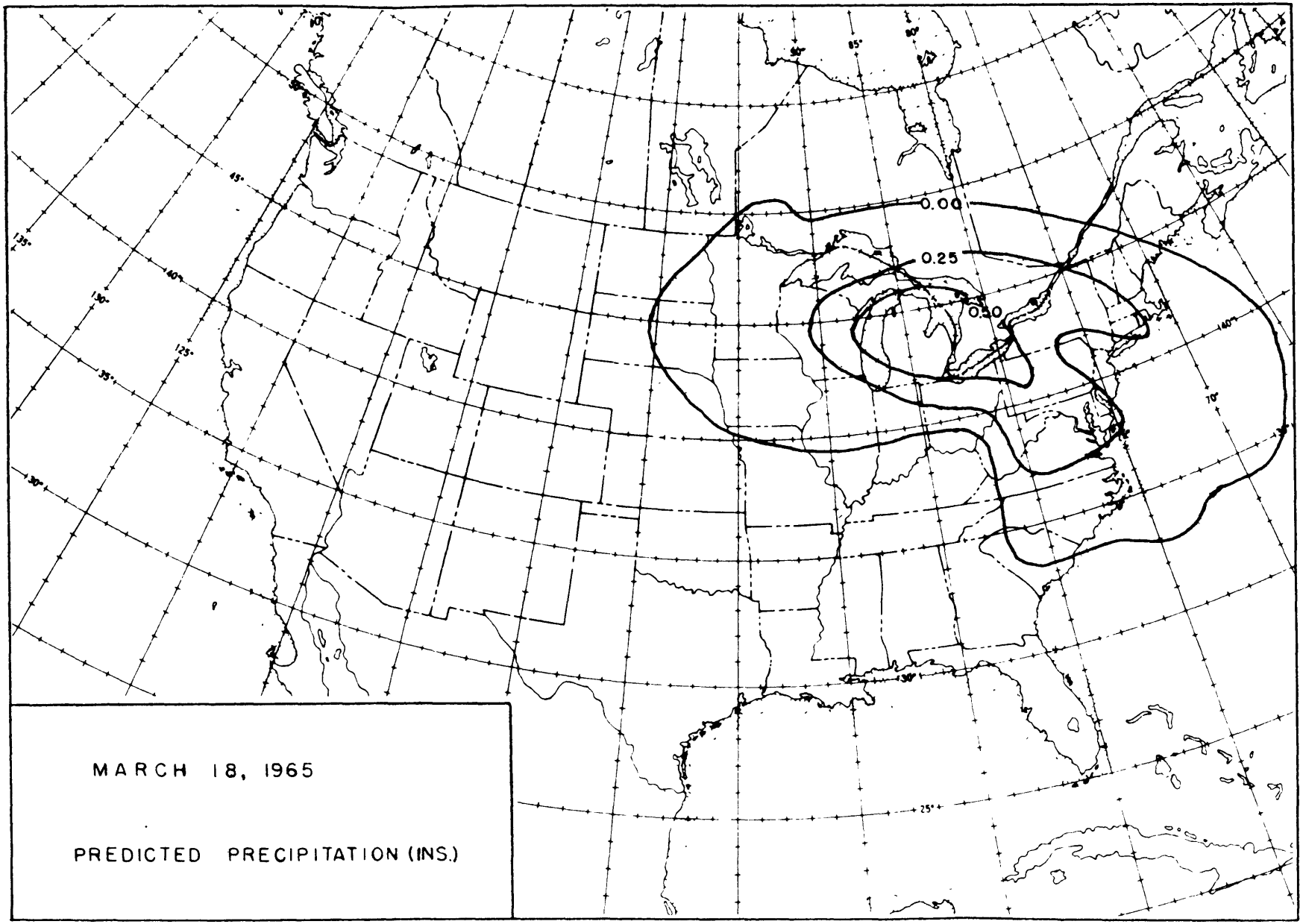

FIGURE 19

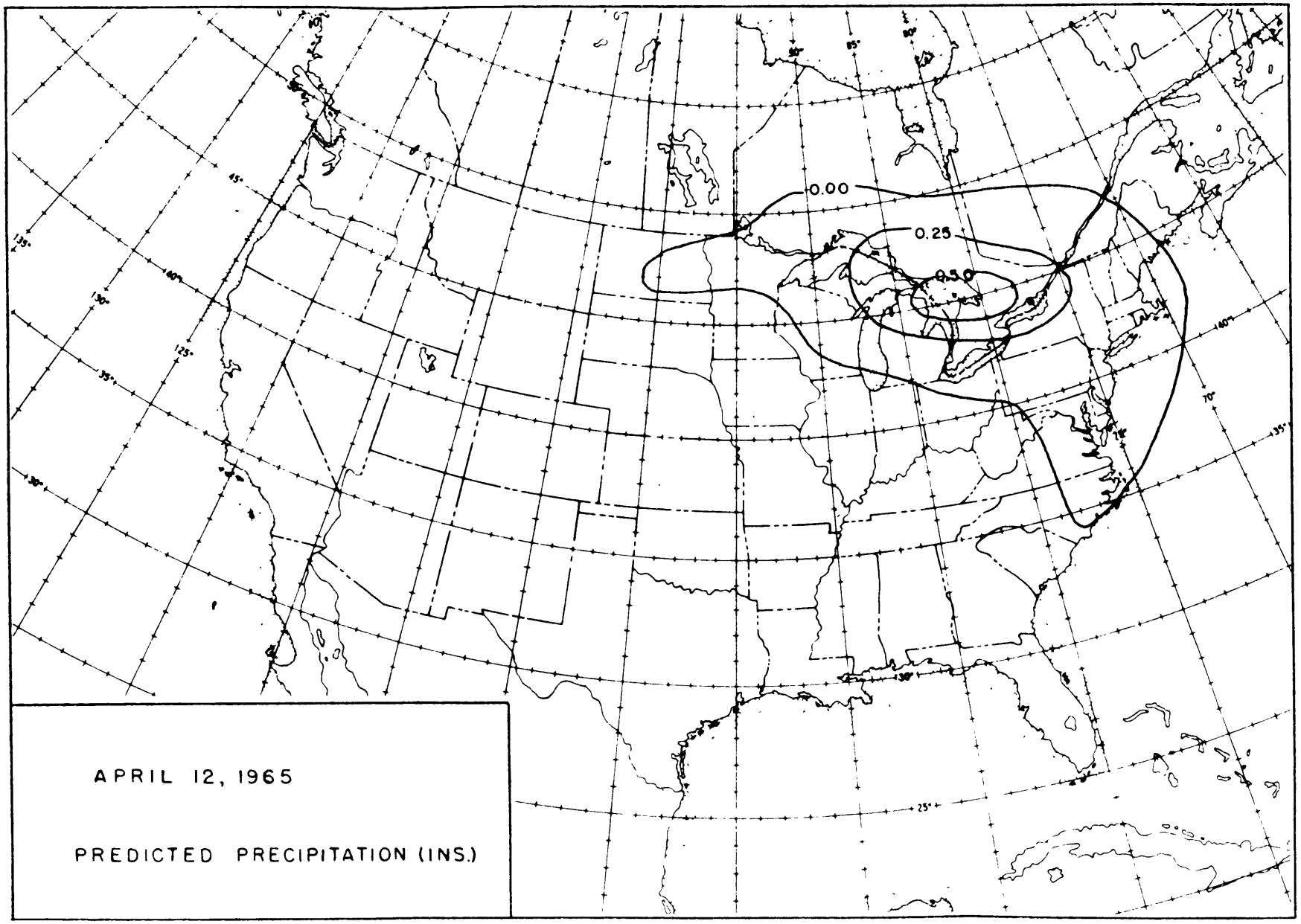

FIGURE 20

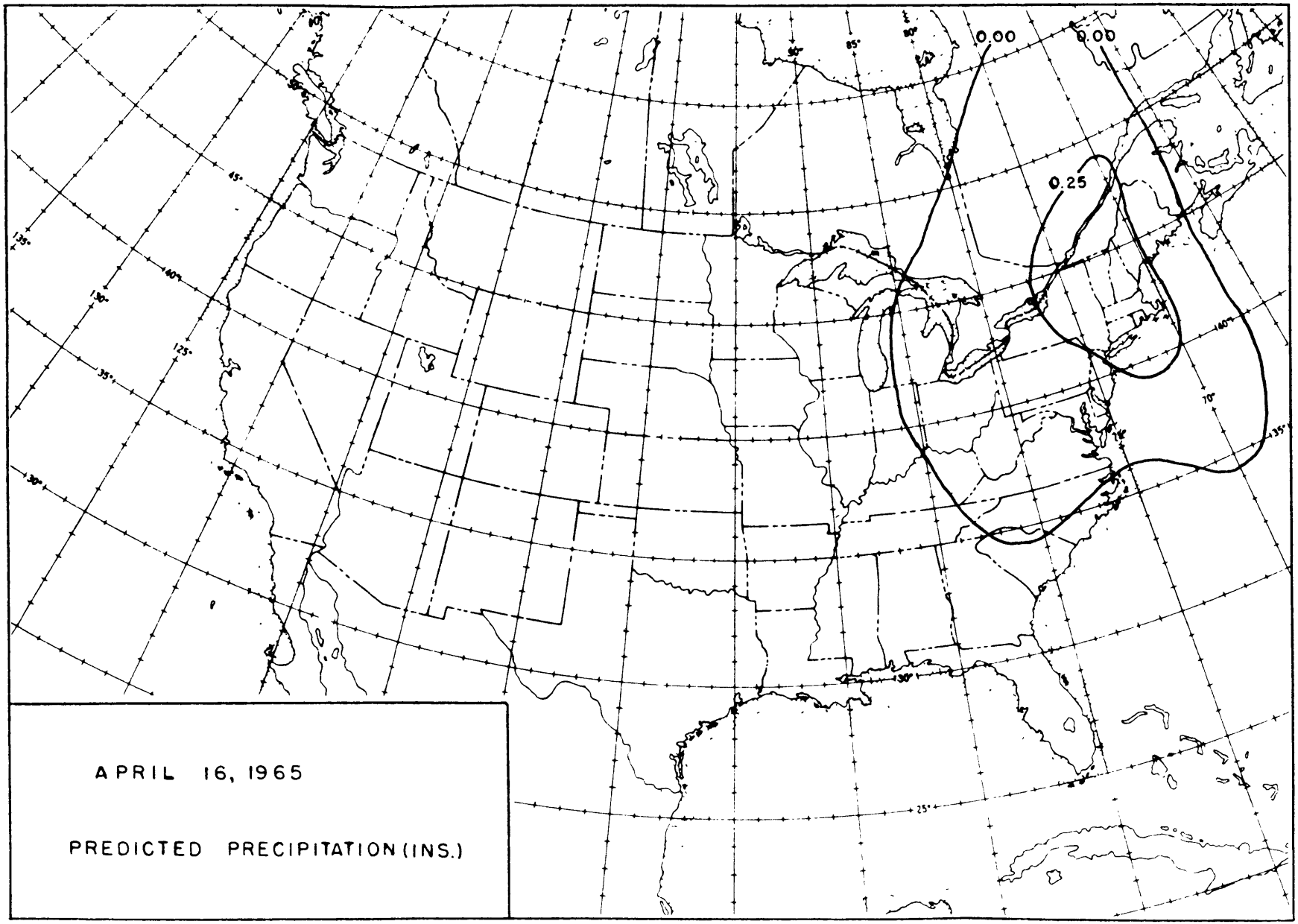

FIGURE 21

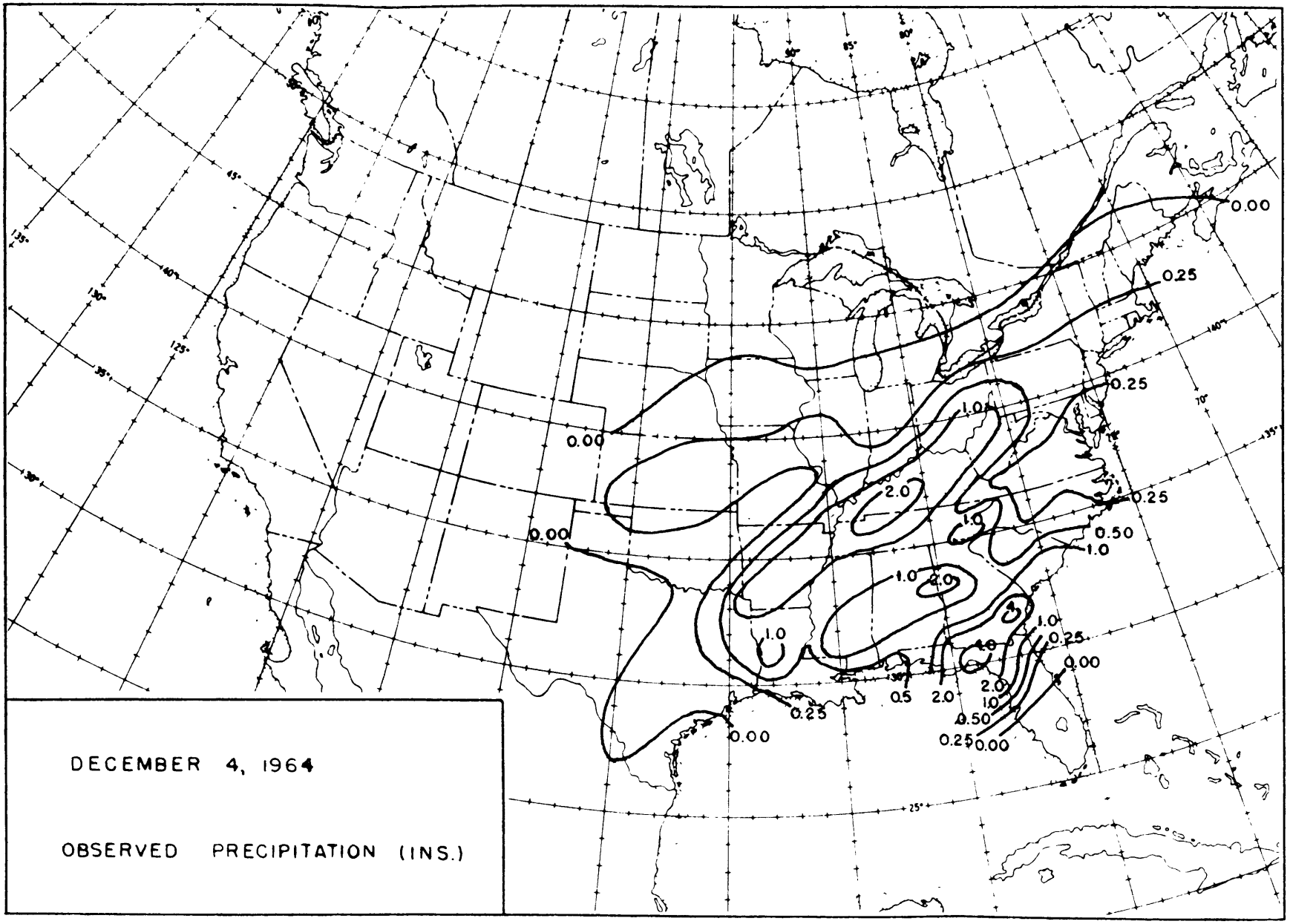
DECEMBER 4, 1964
OBSERVED PRECIPITATION (INS.)
0.00
0.25
0.25
1.0
0.00
2.0
0.25
1.0
0.50
1.0
1.0
2.0
1.0
1.0
0.25
0.00
2.0
1.0
0.50
0.25
0.00
0.25
0.5
2.0
0.00

FIGURE 22

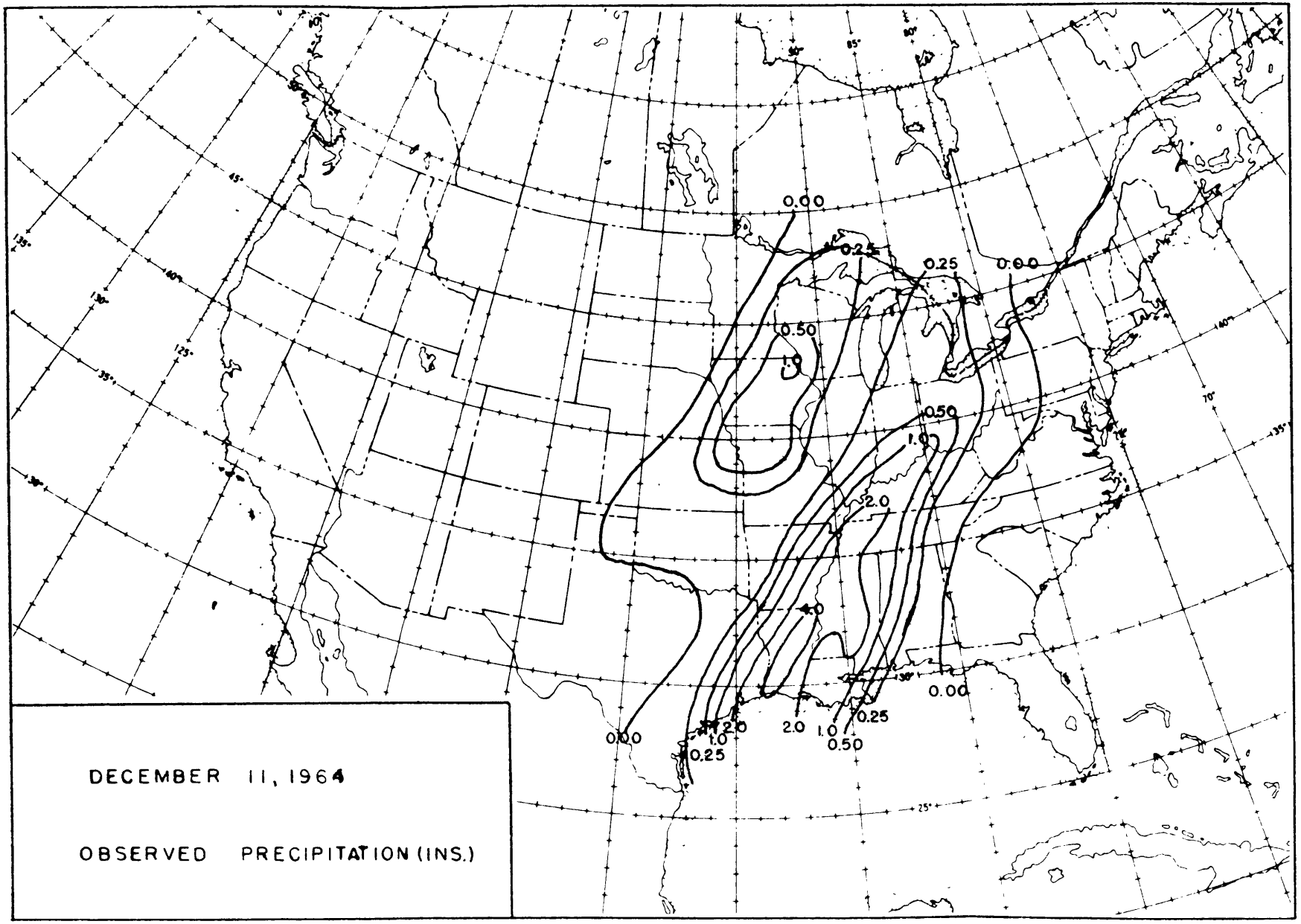
0.00
0.25
0.25
0.00
0.50
1.0
0.50
1.0
2.0
4.0
0.00
0.00
2.0
1.0
0.25
0.25
1.0
0.50
DECEMBER 11, 1964
OBSERVED PRECIPITATION (INS.)

FIGURE 23

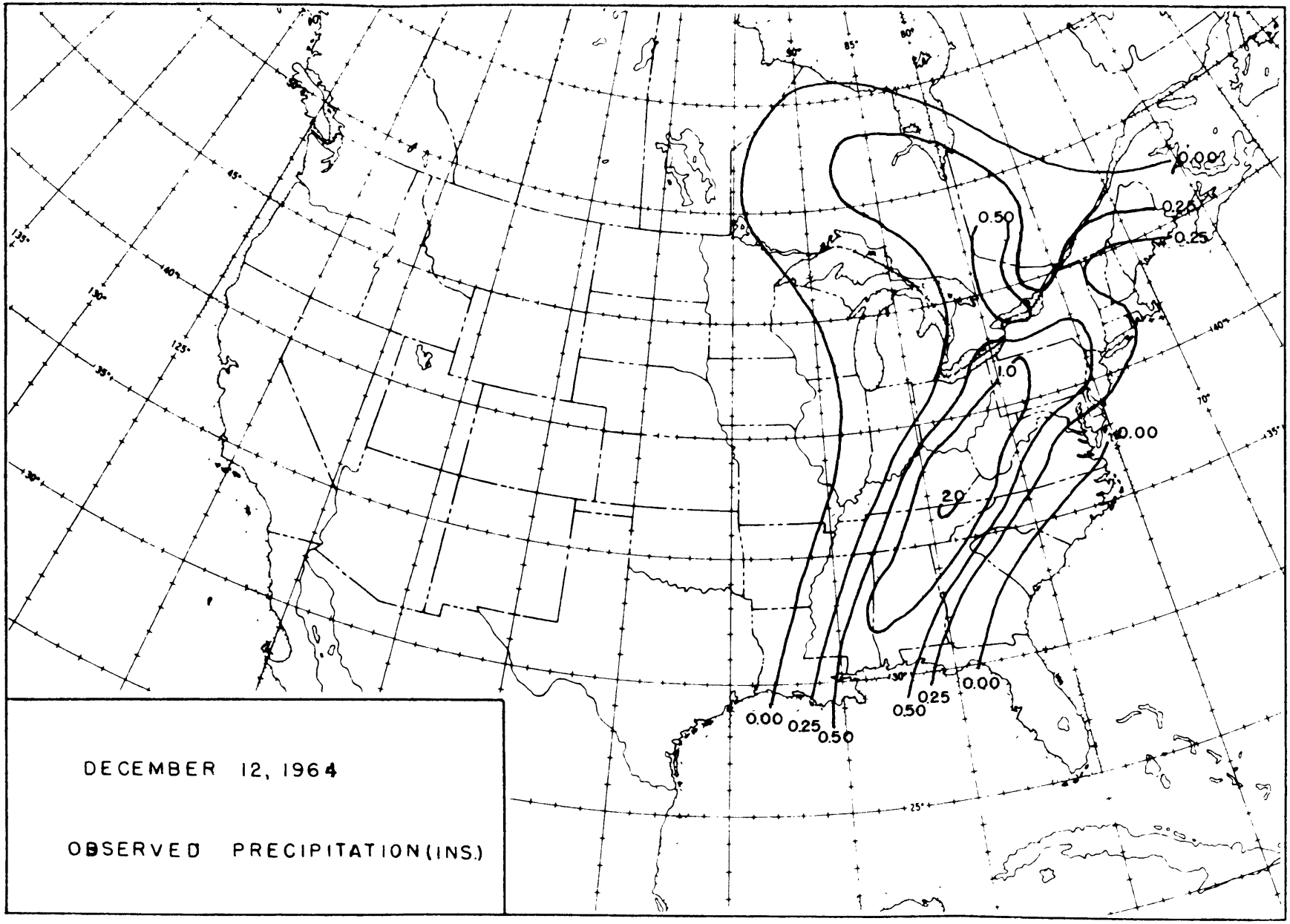
0.00
0.25
0.50
1.0
2.0
0.00
0.25
0.50
0.00
0.25
0.50
0.00
DECEMBER 12, 1964
OBSERVED PRECIPITATION (INS.)

FIGURE 24

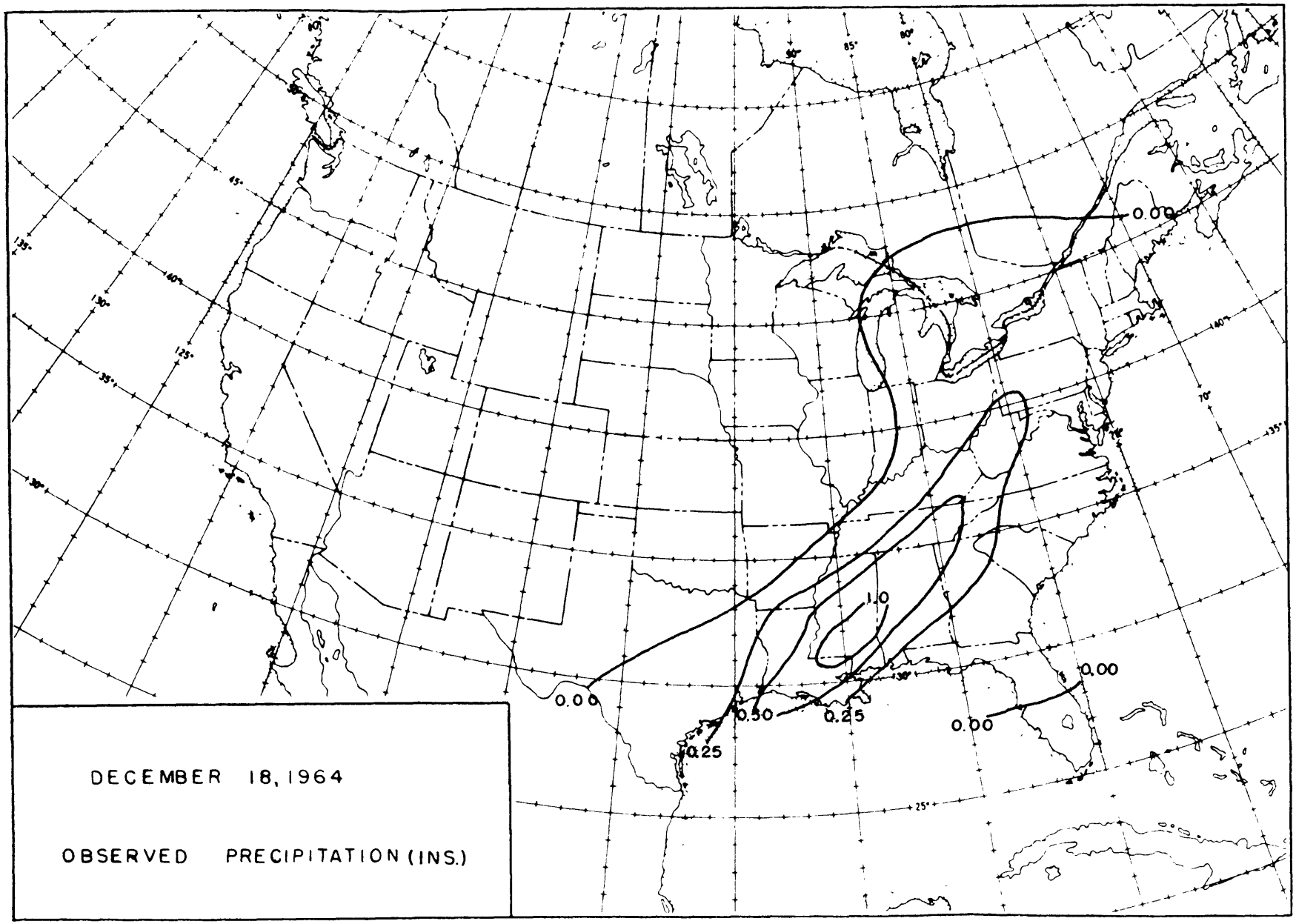
DECEMBER 18, 1964
OBSERVED PRECIPITATION (INS.)
0.00
0.00
1.0
0.00
0.00
0.50
0.25
0.25

FIGURE 25

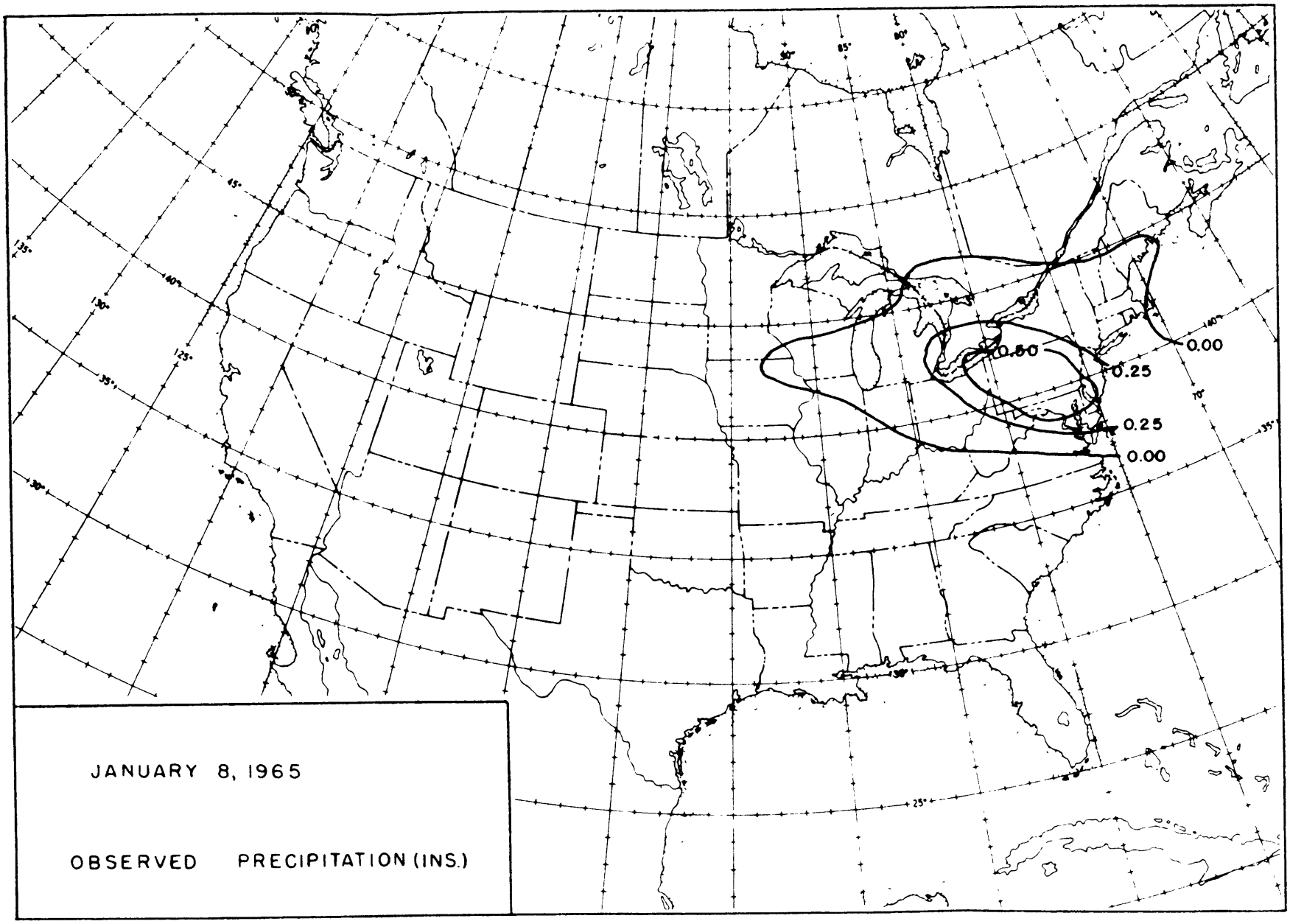
0.50
0.25
0.25
0.00
0.00
JANUARY 8, 1965
OBSERVED PRECIPITATION (INS.)

FIGURE 26

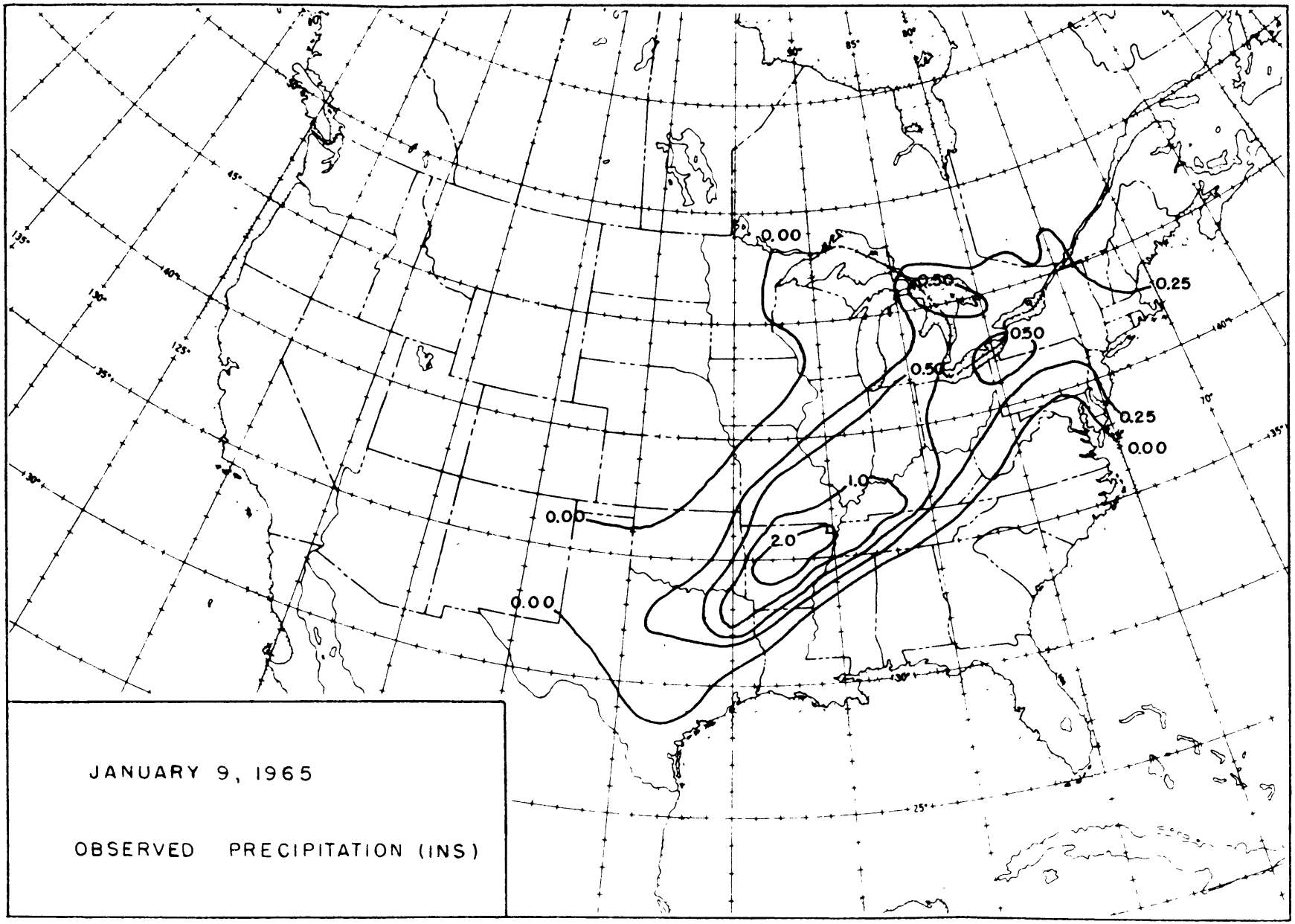
0.00
0.50
0.25
0.50
0.50
0.25
0.00
1.0
0.00
2.0
0.00
JANUARY 9, 1965
OBSERVED PRECIPITATION (INS)

FIGURE 27

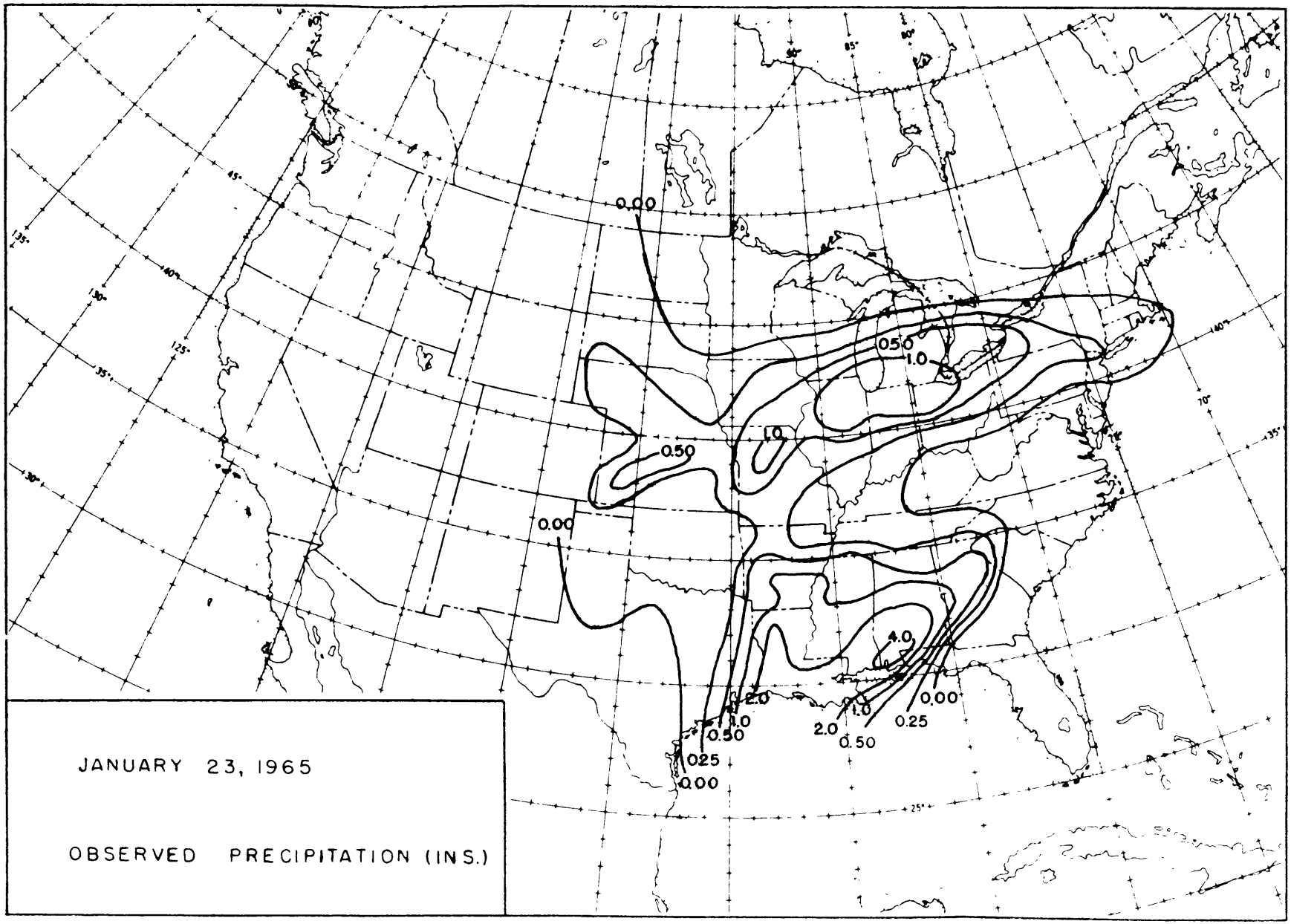
0.00
0.50
1.0
0.50
1.0
0.00
4.0
2.0
1.0
0.50
0.25
2.0
1.0
0.50
0.25
0.00
0.00
JANUARY 23, 1965
OBSERVED PRECIPITATION (INS.)

FIGURE 28

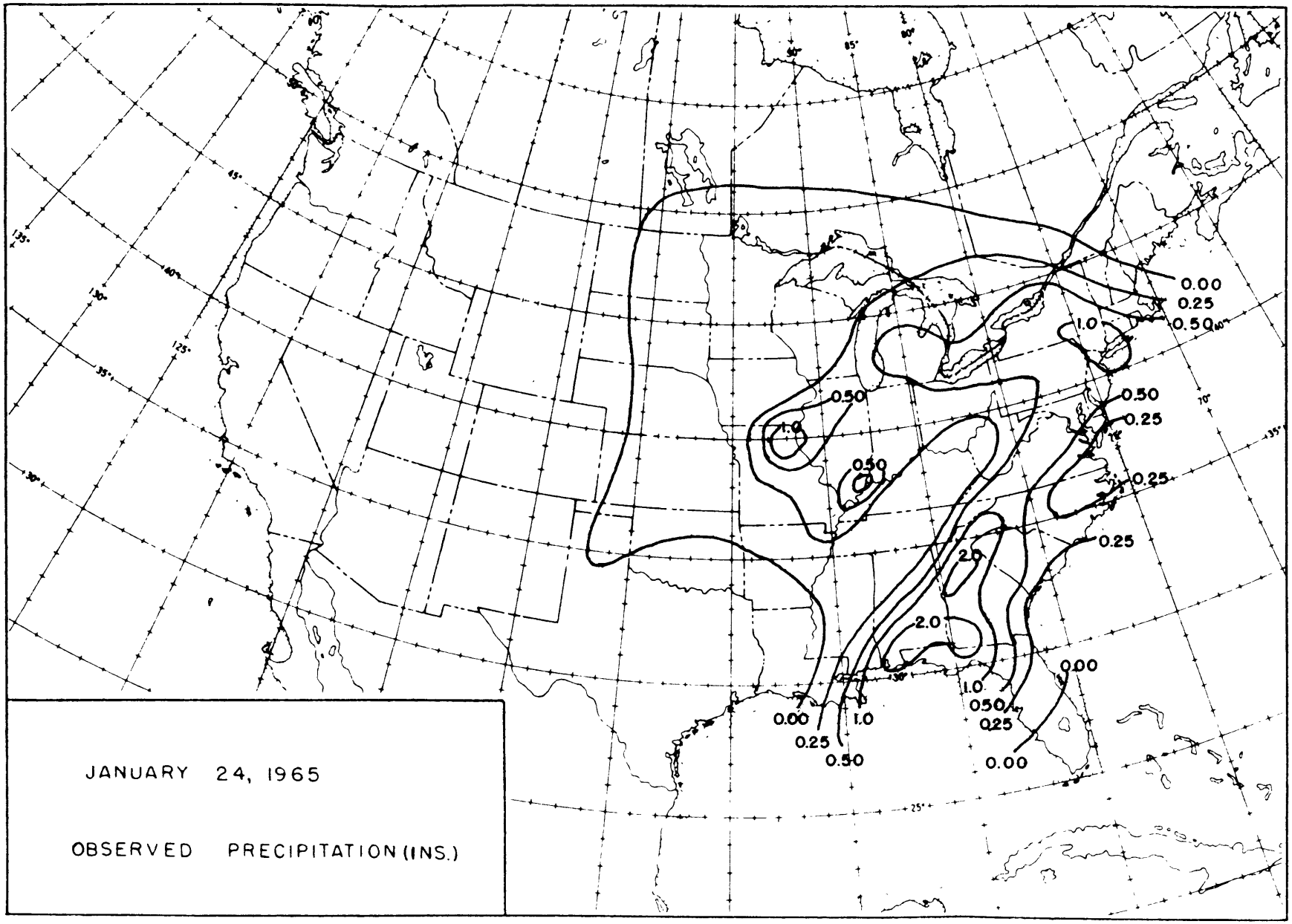
JANUARY 24, 1965
OBSERVED PRECIPITATION (INS.)
0.00
0.25
0.50
1.0
2.0

FIGURE 29

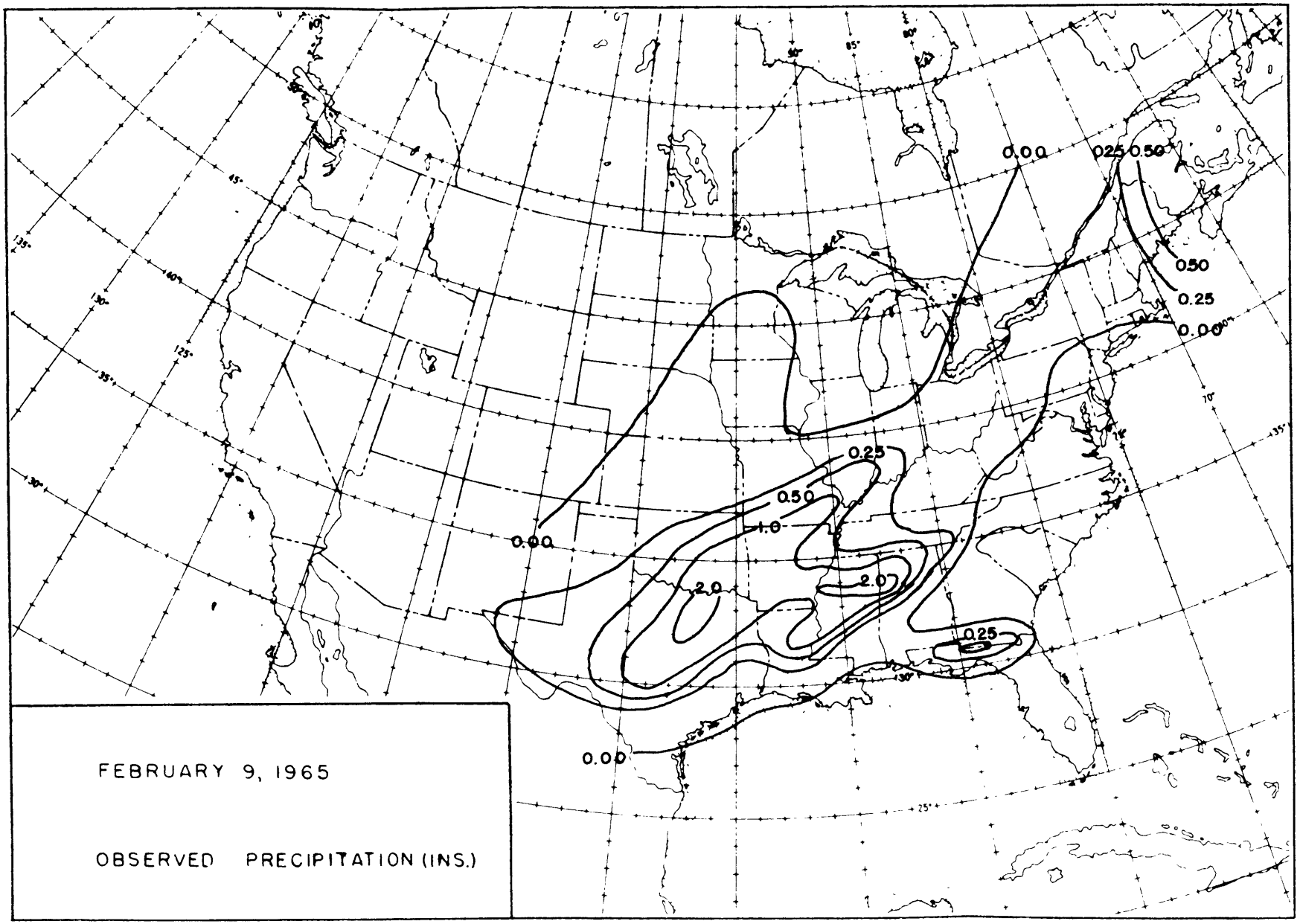
0.00
0.25
0.50
0.50
0.25
0.00
0.25
0.50
1.0
0.00
2.0
2.0
0.25
0.00
FEBRUARY 9, 1965
OBSERVED PRECIPITATION (INS.)

FIGURE 30

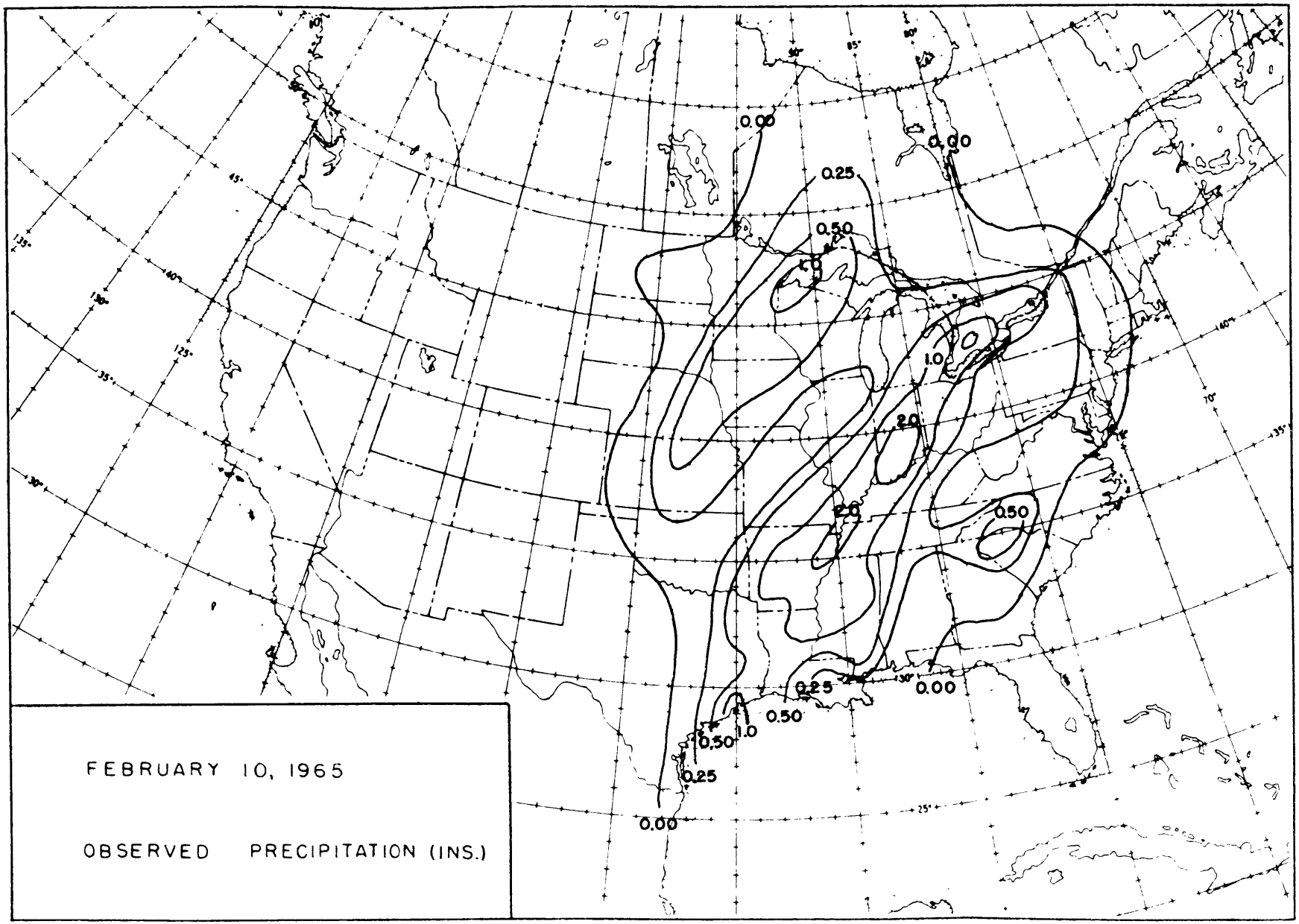
0.00
0.00
0.25
0.50
1.0
1.0
2.0
2.0
0.50
0.25
0.00
0.50
1.0
0.50
0.25
0.00
FEBRUARY 10, 1965
OBSERVED PRECIPITATION (INS.)

FIGURE 31

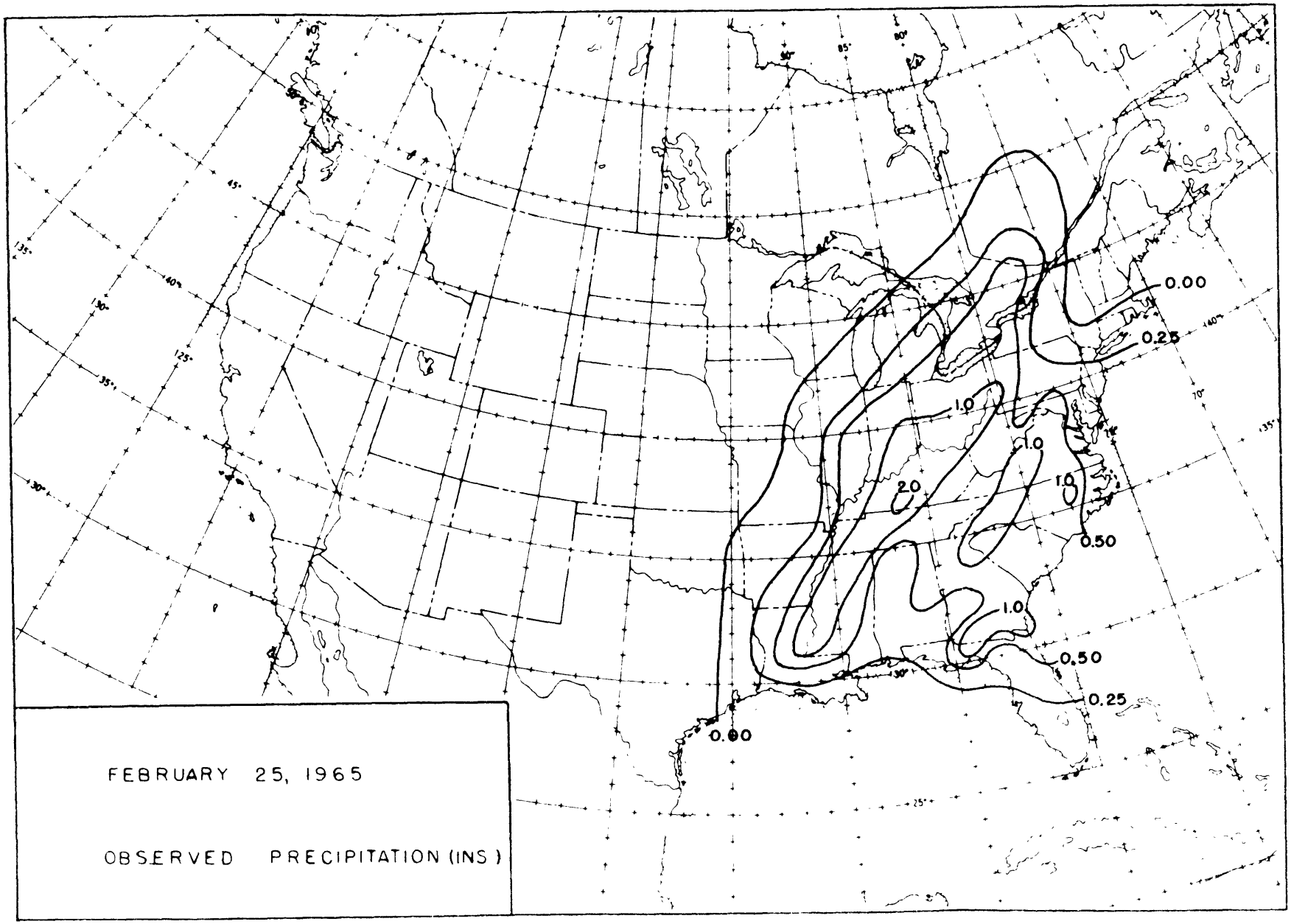
0.00
0.25
1.0
1.0
1.0
2.0
0.50
1.0
0.50
0.25
0.00
FEBRUARY 25, 1965
OBSERVED PRECIPITATION (INS)

FIGURE 32

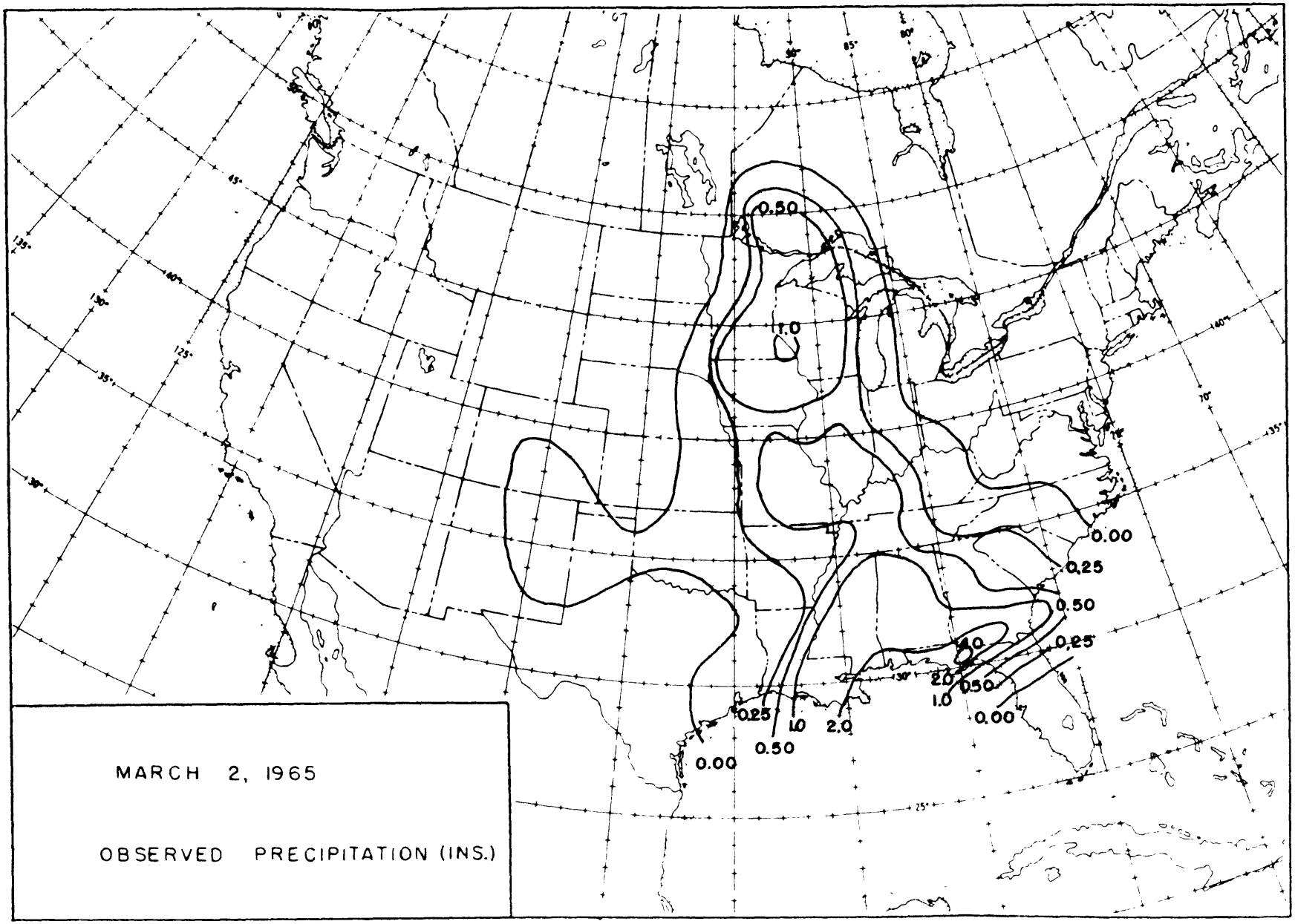
MARCH 2, 1965
OBSERVED PRECIPITATION (INS.)
0.50
1.0
0.00
0.25
0.50
1.0
0.25
2.0
1.0
0.50
0.00
0.25
1.0
2.0
0.50
0.00

FIGURE 33

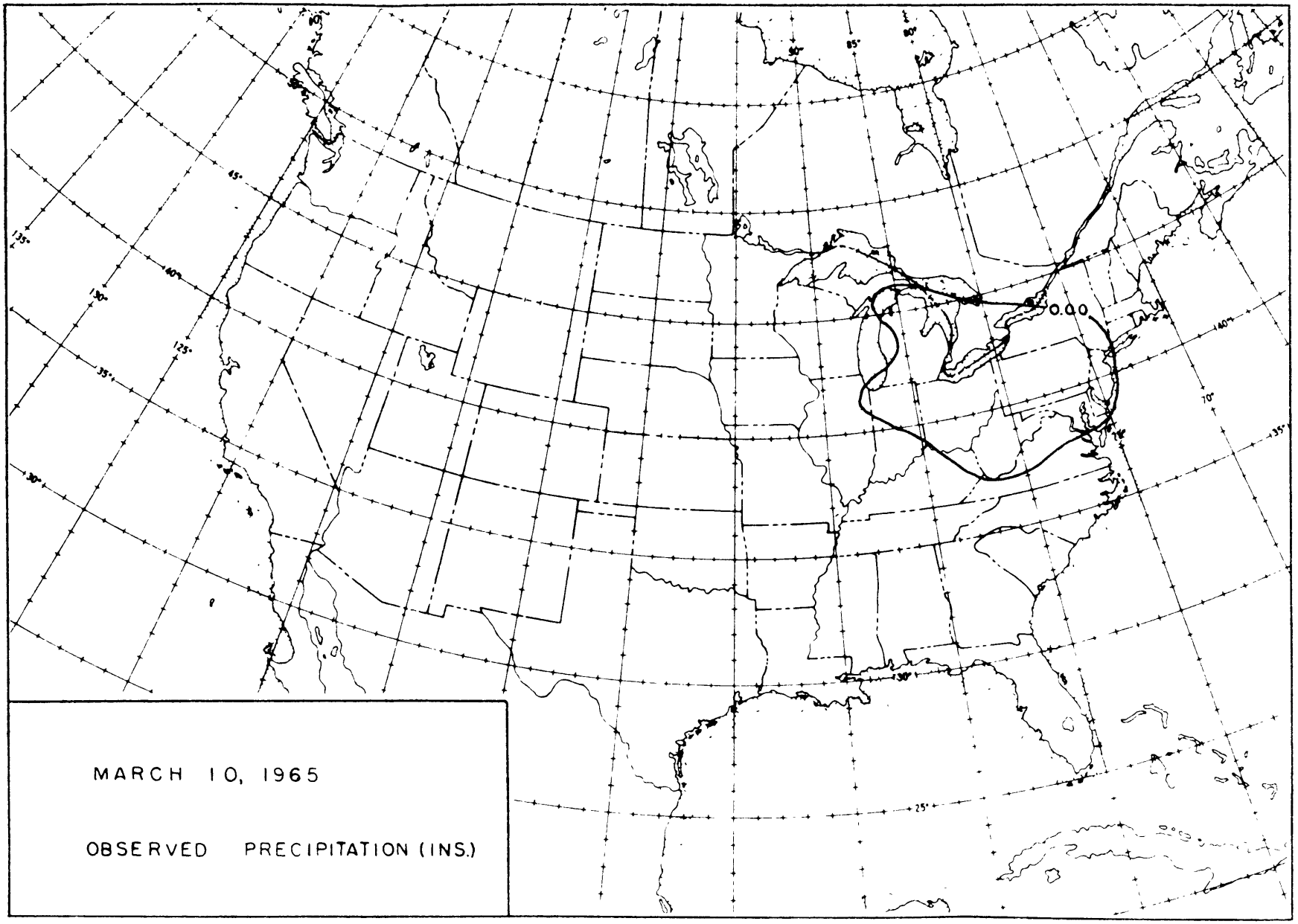

FIGURE 34

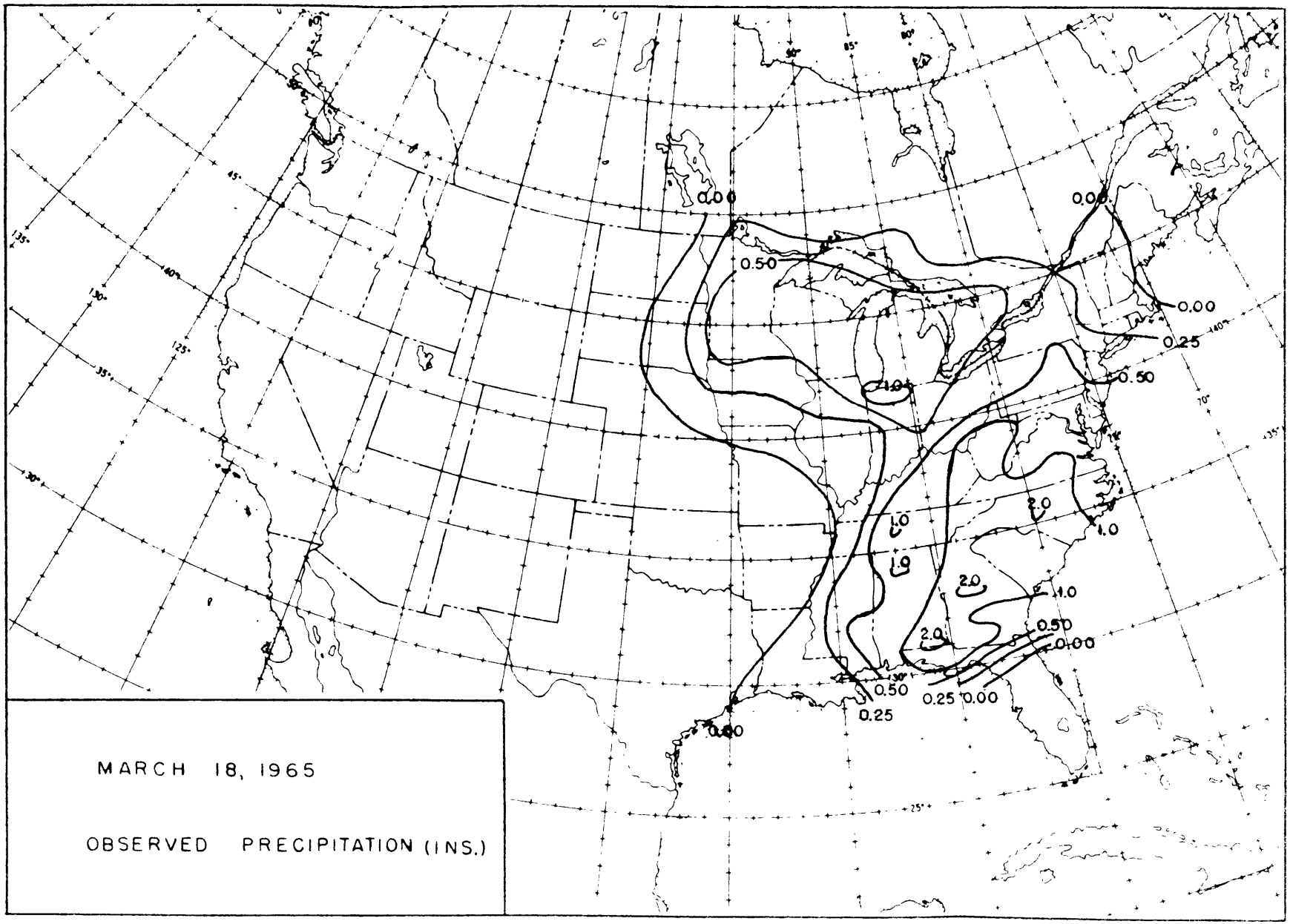

FIGURE 35

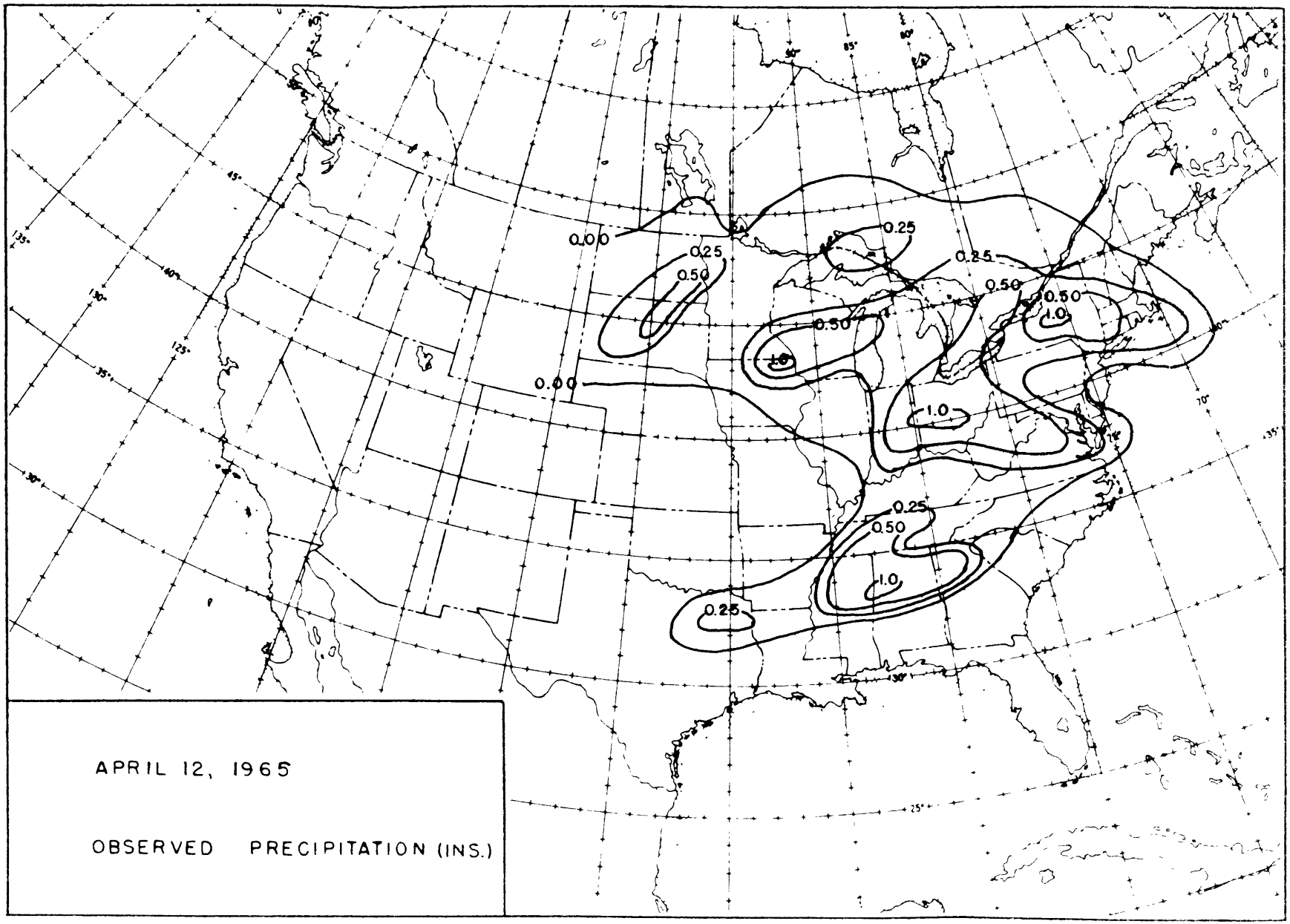

FIGURE 36

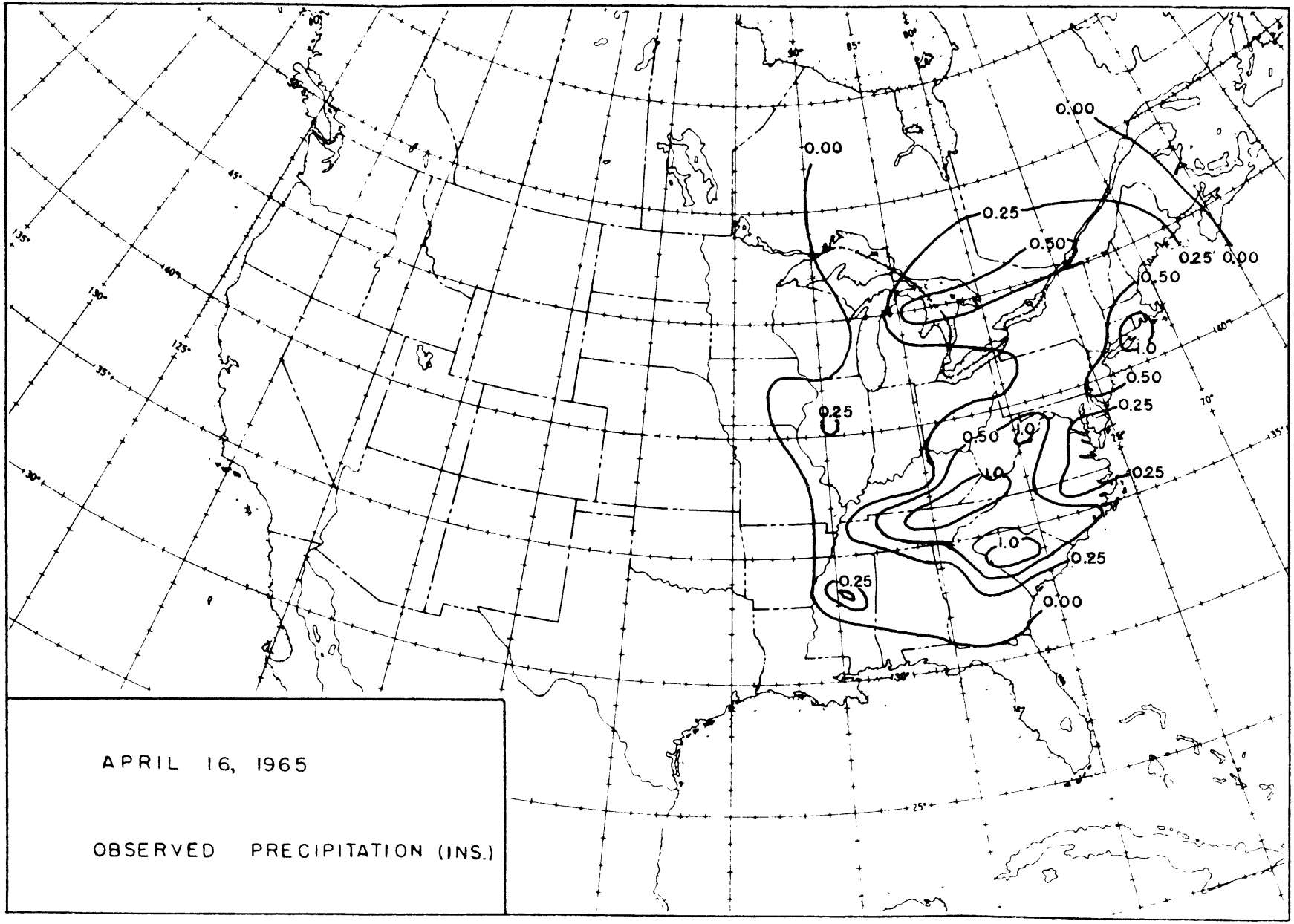

FIGURE 37